MARMARA UNIVERSITY

INSTITUTE FOR GRADUATE STUDIES

INVESTIGATION OF THE PARALLELIZATION OF GREEN'S FUNCTION METHOD FOR HIGH-ORDER HARMONIC GENERATION SIMULATIONS

GÖKHAN İLHAN

MASTER THESIS

Department of Physics

Thesis Supervisor

Prof. Dr. Erdi Ata BLEDA

ISTANBUL, 2023

MARMARA UNIVERSITY

INSTITUTE FOR GRADUATE STUDIES

INVESTIGATION OF THE PARALLELIZATION OF GREEN'S FUNCTION METHOD FOR HIGH-ORDER HARMONIC GENERATION SIMULATIONS

GÖKHAN İLHAN

(521219003)

MASTER THESIS

Department of Physics

Thesis Supervisor

Prof. Dr. Erdi Ata BLEDA

ISTANBUL, 2023

MARMARA UNIVERSITY
INSTITUTE FOR GRADUATE STUDIES IN PURE AND APPLIED SCIENCES

Gökhan İLHAN, a Master of Science of Philosophy student of Marmara University Institute for Graduate Studies in Pure and Applied Sciences, defended his thesis entitled "**Investigation of the Parallelization of Green's Function Method For High-Order Generation Simulations**", on and has been found to be satisfactory by the jury members.

Jury Members

Prof .Dr. Erdi Ata Bleda (Advisor)

Marmara University ..... (SIGN) .....

Prof. Dr. Mustafa Alevli (Jury Member)

Marmara Üniversitesi ..... (SIGN) .....

Assist. Prof. Dr. Emrah Koç (Jury Member)

İstanbul Arel University ..... (SIGN) .....

APPROVAL

Marmara University Institute for Graduate Studies in Pure and Applied Sciences Executive Committee approves that Gökhan İLHAN be granted the degree of Master of Science of Philosophy in Department of Physics, Physics Program on . (Resolution no:).

Director of the Institute

ACKNOWLEDGEMENT

I would like to thank esteemed Prof. Dr. Erdi Ata BLEDA, who helped me throughout my graduate studies and my thesis. His guidence was invaluable for the successful completion of this thesis. I will always make an example of his teachings throughout my life.

I also want to to thank my family for their unwavering support throughtout my education life.

Finally, I would like to extend my thanks to all the faculty members in the Department of Physics at Marmara University.

January 2023 **Gökhan İLHAN**

TABLE OF CONTENTS

ACKNOWLEDGEMENT i
TABLE OF CONTENTS ii
ÖZET iii
ABSTRACT iv
SYMBOLS v
ABBREVIATIONS vi
LIST OF FIGURES vii
LIST OF TABLES viii
1. INTRODUCTION 1
2. THEORY 3
2.1. Time Evolution 3
2.1.1. Schrödinger's Picture: 4
2.1.2. Heisenberg's Picture: 4
2.1.3. Interaction Picture (Also known as Dirac's Picture): 4
2.2. Time Dependent Perturbation 9
2.3. Green's Function 10
2.4. Simulation 14
2.5. Power Spectrum 19
2.6. Notes on Parallelization 20
3. RESULTS AND DISCUSSIONS 21
3.1. Simulation 21
3.2. Some Thoughts on Error Propagation 25
3.3. Parallelization 25
3.4. Pseudo Code 26
4. CONCLUSION 27
REFERENCES 28
ÖZGEÇMİŞ 30

ÖZET

GREEN FONKSİYONU YÖNTEMİNİN YÜKSEK MERTEBELİ HARMONİK ÜRETİM SİMÜLASYONLARI İÇİN PARALELİZASYONUNUN İNCELENMESİ

Yüksek mertebeli harmonik üretimi (YHÜ), femtosaniye atma süresine sahip şiddetli bir lazer alanını bir gaz hedefine odaklayarak aşırı ultraviyole (XUV) bölgede ışık üreten doğrusal olmayan bir süreçtir. Sürücü lazer alanı genellikle birkaç femtosaniye atma süresine sahip olup, şiddeti TW/cm^2 mertebesindedir. Çok sayıda lazer fotonunu yüksek enerjili tek bir fotona dönüştürmenin bu doğrusal olmayan sürecine YHÜ denir. Bir frekans dönüştürme süreci olarak temel doğasının yanı sıra, YHÜ, hedefin yapısı hakkında ultra hızlı (ottosaniye mertebeli) bir zaman ölçeğinde bilgi elde etmek için bir yöntem olarakta ilgi görmeye devam etmektedir.

YHÜ sürecinde, plato bölgesinde yayılan fotonların, hem şiddetlerini artırmak hem de kesme frekansını uzatmak onlarca yıldır bilimsel araştırmaların odak noktasında yer almıştır. Böyle bir gelişimi başarmanın bir yolu, serbest hedefi homojen olmayan bir bölgeye yerleştirmektir. Arzu edilen iyileştirmeye ulaşmanın bir başka yolu ise, hedefin hapsedilmesidir (mesela C_{60} kafesi içine). Topçu ve çalışma arkadaşları C_{60} kafesine kapatılmış bir hidrojen atomundan YHÜ sürecini incelemiştir. Bu tür sistemlerde, lazer şiddetinin YHÜ'ne yönelik yanıt almaya yetecek, ancak iyonizasyon yoluyla Coulomb patlaması nedeniyle kafesi kıracak kadar güçlü olmayacak bir düzeye düşürülmesi gerekir. 3-boyutlu Zamana Bağlı Schrödinger'in Denklemi (ZBSD)'ni çözmek, bu sistemin gelişim sürecini yöneten dinamiklerin analizi konusunda sınırlayıcı kalmaktadır. Bunun temel nedeni, atomun lazerle etkileşimi sırasında ekseriyetli olarak başlangıç durumunda kalmasıdır. Bu tür sistemlerde vukuu bulan temel süreçleri analiz etmek için, pertürbatif yöntemlerin kullanımı gerekmektedir. Bu yöntemlerden biri de zamana bağlı pertürbasyon teorisi çerçevesindeki Green fonksiyonu yöntemidir. Dalga fonksiyonunun ilk hali altında gömülü ve saklı kalmış dinamikleri, zamanın bir fonksiyonu olarak dalga fonksiyonuna ihtiyaç duyulan mertebede yapılacak düzeltmelerin analizi ile çıkarılabilir.

Bu tür simülasyonların seri uygulamaları genelde 5-6 saate kadar CPU zamanı alabilmektedir. Önceki çalışmada gösterilmiştir ki YHÜ simülasyonlarında, uygun paralelleştirme ile ciddi hız kazanımları elde etmek mümkündür. Bu tezde, ilk aşamada Green fonksiyonları ile $n.$ mertebe zamana bağlı pertürbasyon teorisini kullanarak YHÜ için paralel zaman yayıcımızın matris denklemlerini geliştirdik ve ardından YHÜ'ni simüle etmek için *OpenMP* API'lerini kullanarak C programlama dilinde paralel bir kod yazdık. Ürettiğimiz sonuçları ZBSD sonuçları ile kıyasladığımızda sonuçlarımızı oldukça tutarlı bulduk.

ABSTRACT
INVESTIGATION OF THE PARALLELIZATION OF GREEN'S FUNCTION METHOD FOR HIGH-ORDER HARMONIC GENERATION SIMULATIONS

High-order harmonic generation (HHG) is a non-linear process that produces coherent extreme ultraviolet (XUV) light by focusing an intense femtosecond laser onto a gas target. The driving laser field is usually at the order of TW/cm^2 with few femtosecond pulse duration. The non-linear process of transforming a large number of laser photons into single high energy photon is referred to as HHG. Besides its fundamental nature as a process of frequency conversion, high-order harmonic generation attracted interest as a source to obtain information about the structure of the target on an ultrafast (orders of attoseconds) time scale.

Both increasing the intensities and pushing the cut-off of the photons emitted in the plateau region have been in the focus of research for decades. One way of achieving such an enhancement is by means of placing the free target in a nonhomogneous field. Another way of achieving the desired enhancement is by means of confinement of the target. Topcu et al. investigated the HHG from a hydrogen atom confined in a C_{60} cage. In such systems, the laser intensity has to be reduced to a level where it is sufficient enough to get a high-order harmonic response from the atom, but not strong enough to fracture the cage due to coulomb explosion via ionization. Solving the 3-dimensional Time Dependent Schrödinger's Equation (TDSE) is limited in analyzing the dynamics governing the enhancement process of this system. The main reason is that the atom mainly remains in its initial state durring the interaction with the laser. To investigate the underlying processes going on in such systems, perturbative methods need to be invoked. One of those methods is the Green's function method in the framework of time dependent perturbation theory. The underlying dynamics hidden beneath the initial state can be extracted by analyzing the desired order of correction to the wavefunction as a function of time.

Serial implementations of such simulations usually take up to 5-6 hours of CPU time. In previous work, it is shown that significant improvement can be achieved in HHG simulations if proper parallelization is achieved. In this master thesis, we first developed the matrix equations for our parallel propagator for the HHG using the n^{th} order time dependent perturbation theory with Green's function method, and then developed a parallel code in C programming language using *OpenMP* APIs to simulate HHG that can handle up to the desired perturbation order n. We found the results of our code to be consistent with the results obtained from TDSE.

SYMBOLS

$\boldsymbol{\omega_0}$: Frequency of Driving Laser

$\widehat{\boldsymbol{H}}$: Time Dependent Total Hamiltonian

$\boldsymbol{\Psi}$: : State Function

$\boldsymbol{\Psi_x^n}$: : n^{th} Order Correction to the State Function in x-representation

$\widehat{\boldsymbol{U}}$: Time Evolution Operator

$\widehat{\boldsymbol{H}}$: Hamiltonian

$\widehat{\boldsymbol{H}}_{\boldsymbol{0,x}}$: Unperturbed Hamiltonian in x-representation

$\widehat{\boldsymbol{H}}_{\boldsymbol{1,x}}$: Interaction Hamiltonian in x-representation

$\widehat{\boldsymbol{H}}_{\boldsymbol{a,x}}$: Atomic Hamiltonian in x-representation (in HHG case)

$\widehat{\boldsymbol{H}}_{\boldsymbol{Int,x}}$: Interaction Hamiltonian in x-representation (in HHG case)

$\boldsymbol{A}$: Transition Amplitude

$\boldsymbol{G}$: Green's Function

$\boldsymbol{L}$: Hermitian Linear Operator

$\boldsymbol{\phi}$: Normalized Eigenfunction

$\boldsymbol{\delta}$: Dirac Delta Function

$\boldsymbol{\theta}$: Heaviside Function

$\boldsymbol{R}$: Radial Part of The Wave Function

$\boldsymbol{U}$: Radial Part of The Wave Function (rR)

$\boldsymbol{\lambda}$: Dimensionless parameter

$\hbar$: Planck's constant

$\boldsymbol{g_{l,i}^{1,k}(\vec{r},t)}$: Intermediate Radial Component Of the Partial Wave Expansion

$\boldsymbol{h_{l,i}^{1,k}(\vec{r},t)}$: Intermediate Radial Component Of the Partial Wave Expansion

$\boldsymbol{Y_l^m(\theta,\phi)}$: Spherical Harmonics

$\boldsymbol{z}$: Complex parameter

$\boldsymbol{z(t)}$: Dipole

$\boldsymbol{\dot{z}(t)}$: Dipole velocity

$\boldsymbol{\ddot{z}(t)}$: Dipole acceleration

$\boldsymbol{E(t)}$: Electric Field

$\boldsymbol{f(t)}$: Laser Profile

$\boldsymbol{S(\vec{r},t)}$: Source Term

$\boldsymbol{P_\mu(\omega)}$: Power Spectrum

ABBREVIATIONS

LASER **:** Light Amplification by Stimulated Emission of Radiation

HHG **:** High-order Harmonic Generation

SPI **:** Single Photon Ionization

MPI **:** Multi-Photon Ionization

ATI **:** Above Threshold Ionization

TI **:** Tunnel Ionization

CUDA **:** Compute Unified Device Architcture

OpenMP **:** Open Multi-Proccessing

LAPACK **:** Linear Algebra Package

TDSE **:** Time Dependent Schrödinger's Equation

FWHM **:** Full Width Half Maximum

LIST OF FIGURES

Figure 1: Diagrammatic representation of the probability amplitude of Dyson series for a transition from..... 8
Figure 2 Driving laser profile. The peak intensity is, $1.0\ x\ 10^{14}\ W/cm^2$ wavelength is 800 nm 22
Figure 3 Comparison of the power spectrum of TDSE (orange curve) with that of the 1st order Perturbation (green curve). 23
Figure 4: Comparison of the power spectrum of TDSE (orange curve) with that of the 4^{th} order Perturbation (green curve). 23
Figure 5: Comparison of the power spectrum of TDSE (orange curve) with that of the 8^{th} order Perturbation (green curve). 24
Figure 6: Ratio of time elapse per perturbation order to TDSE. Trendline is also shown. Each point shown is the outcome of the best of 5. 25

LIST OF TABLES

Table 1: Parameters list of our program..... 21

1. INTRODUCTION

When an atom is exposed to an intense laser field, a time dependent dipole moment is induced. Then it starts to radiate. The photons emitted in such a process are odd multiples of the driving laser frequency ω_0. In 1987, McPherson, et al. [1] observed the 13^{th} harmonic in He, 17^{th} harmonic in Ne, 7^{th} harmonic in Ar and Kr, and finally 9^{th} harmonics in Xe of $248\ nm$. This is the first time this non-linear phenomenon was observed. We should mention that in earlier days, this phenomenon was known as Optical Harmonic Generation (OHG). Franken et al. [2] gives a brief discussion of requisite analysis and a description of the experiments in which they observed second harmonic at $\approx 347\ nm$ when the target was lit by a beam of $\approx 694\ nm$. Advancements in high-power short-pulse laser technologies enabled more observations of high-order harmonic generations (HHG): the presence of higher order harmonics was confirmed by measuring the spatial [3–9] , temporal [10–13], and spectral properties [14–16] of the harmonics in various laboratories.

Intense laser fields also enabled several more mechanisms for ionization besides the well-known single-photon ionization, such as multiphoton ionization (MPI), above threshold ionization (ATI), and Tunneling Ionization (TI). Krause et al. [17] in 1992 and Corkum [18] in 1993 laid down the theoretical foundations of HHG. The theoretical model consists of three steps and it is known as "Simple Man Model" (SMM). In the first step of the model, the laser field suppresses the Coulomb potential allowing the electron to tunnel through. It is assumed that electron reaches the continuum with zero kinetic energy. In the second step, electron is driven in the laser field gaining kinetic energy. In the third and final step, the electron recombines with the parent ion and emits high energy photons. SMM is even further improved by Ivanov et.al. [19], recently.

HHG process enables the generation of coherent extreme ultraviolet (XUV) radiation, which is then used to attain isolated pulses with durations at the order of tens of attoseconds [20]. Attosecond time scale is the natural time scale in atomic physics. Increasing the yield of HHG is still an active area of research. One way of achieving this is by changing the environment of the target, such as placing the target in a non-homogenous field [21–26] or, as another way, by confining the target [27–30]. Topcu et al. [30] investigated HHG from a hydrogen atom confined in a C_{60} cage. They noted that the laser intensity must be strong enough to get a high-order harmonic response from the hydrogen atom, but at the same time, weak enough not to break the cage due to the coulomb explosion by ionization. Solving the Time Dependent Schrödinger's Equation (TDSE) is limited in analyzing the dynamics governing this process due to the fact that the target atom essentially remains in its initial state during its interaction with the laser field. The useful information is embedded beneath the initial state which requires perturbative methods to extract the relevant information to investigate the underlying dynamics going on in such systems. Time dependent perturbation theory provides a framework as time dependent corrections to the unperturbed Hamiltonian. From

mathematical point of view, time dependent perturbation theory provides inhomogeneous differential equations. One of the most systematic approaches of solving inhomogeneous differential equations is the use of Green's functions [31,32]. The theoretical foundations of Green's functions and their connection to perturbative approaches in HHG are established in the *Theory* section of this thesis. In Ozan OĞUZ's work [33], significant improvement is achieved when HHG simulations are parallelized. With this motivation, after establishing the theoretical foundations, we investigated possible mechanisms of parallelization. We developed an *OpenMP* based parallel C code to simulate HHG within the framework of n^{th} order perturbation theory using Green's function method. In the *Results and Discussions* chapter, we compared the results obtained directly from the solution of Time Dependent Schrödinger Equation (TDSE). At the end of that section, we provided a pseudo code showing one of the parallelization schemes.

2. THEORY

When the laser intensity is at the order of $10^{15} - 10^{18}\ W/cm^2$ at its peak, the electric field component of the laser field is strong enough to suppress the Coulomb potential which renders the approximate methods ineffective in simulating the interaction of the laser field with a free target. However, in the case of confined target, the story is little different. The high-order harmonic generation from a hydrogen atom confined in a fullerene can be given as an example [34] . In the simulations of such confined systems, the laser intensities should be strong enough to generate high-order harmonics, but weak enough not to damage the confining cage. Such intensities unfortunately leave the target primarily in the initial state, making the analysis of the propagated wave function very difficult. The useful information is embedded beneath the initial wave function which can be extracted by the time dependent perturbation theory. In this section we introduce the Green's function formalism for the n^{th} order time dependent perturbation theory and its parallel implementation.

2.1.Time Evolution

The time dependent wave function of a system can be obtained from the Time Dependent Schrödinger Equation (TDSE)

$$i\hbar \frac{\partial \Psi(\vec{r},t)}{\partial t} = \hat{H}\Psi(\vec{r},t), \tag{1}$$

where $\hat{H}$ is the Hamiltonian describing the system. The solution to this differential equation needs to satisfy the given initial state $\Psi(\vec{r},t)$ at $t = t_0$. If we apply the separation of variables method and substitute the solution $\Psi(\vec{r},t)$ expressed as a product of $\Psi(t)$ and $\Psi(\vec{r},t_0)$ in Eq.1, we obtain the solution

$$\Psi(\vec{r},t) = \exp\left[-\frac{i}{\hbar}\int_{t_0}^{t} \hat{H}\, dt\right]\Psi(\vec{r},t_0). \tag{2}$$

We call the operator

$$\hat{U}(t,t_0) = \exp\left[-\frac{i}{\hbar}\int_{t_0}^{t} \hat{H}\, dt\right] \tag{3}$$

time evolution operator. It should be clear from the definition that

$$\hat{U}(t_0,t_0) = \hat{I}, \tag{4}$$

where $\hat{I}$ is the identity operator. We need to mention that when the Hamiltonian is time dependent, care must be taken in Eq.3 for its validity. Generally, $\frac{d}{dt}e^{\hat{A}(t)}$ is not equal to $\frac{d\hat{A}}{dt}e^{\hat{A}(t)}$.

Before we move onto more practical use of Eq.3, let's discuss pictures in quantum mechanics first:

2.1.1. Schrödinger's Picture:

In Schrödinger's picture, the operators are mostly time independent. The time dependence of a quantum state is carried out on the state vector itself. If we depict an operaor in Schrödinger's picture as a time independent operator $\hat{A}_S$, the time dependence is carried out on the state vector as

$$|\Psi(t)\rangle = \hat{U}(t, t_0)|\Psi(t_0)\rangle \tag{5}$$

in bra-ket notation. The expectation value is then

$$\langle \hat{A}_S(t)\rangle = \langle \hat{U}(t, t_0)\Psi(t_0)|\hat{A}_S|\hat{U}(t, t_0)\Psi(t_0)\rangle \tag{6}$$

2.1.2. Heisenberg's Picture:

In Heisenberg's picture, unlike Schrödinger's picture, the state vectors are independent of time. The time dependence is carried out on the operators. If an operator in Heisenberg's picture is depicted as $\hat{A}_H(t)$, it is written as

$$\hat{A}_H(t) = \hat{U}^\dagger(t, t_0)\hat{A}_S\hat{U}(t, t_0) \tag{7}$$

whereas the state vectors is simply $|\Psi(\vec{r}, t_0)\rangle$. The expectation value is

$$\langle \hat{A}_H(t)\rangle = \langle \Psi(t_0)|\hat{U}^\dagger(t, t_0)\hat{A}_S\hat{U}(t, t_0)|\Psi(t_0)\rangle \tag{8}$$

2.1.3. Interaction Picture (Also known as Dirac's Picture):

Although the expectation values are the same in all pictures, their use in quantum mechanics improves the mathematical formulation in certain cases. In interaction picture, both the operators and the state vectors carry some part of the overall time dependence. This is particularly useful if the interaction term in the Hamiltonian can be seperated from the part of the Hamiltonian which can be solved exactly, so that we can write the Hamiltonian as $\hat{H}_S = \hat{H}_{0,S} + \hat{H}_{1,S}$. Here, S represents that the operators are expressed in Schrödinger's picture, 0 indicates the part of the Hamitonian that can be solved exactly and 1 indicates the interaction part of the Hamitonian (say, for example with the external field). This representation will be adopoted later in this work when dealing with time dependent perturbation theory.

In the interaction picture, the time dependent state function is written as

$$|\Psi_I(t)\rangle = \exp\left(\frac{i}{\hbar}\hat{H}_{0,S}(t - t_0)\right)|\Psi_S(t)\rangle, \tag{9}$$

where $|\Psi_S(t)\rangle = \exp\left[-\frac{i}{\hbar}\hat{H}_S(t - t_0)\right]|\Psi(t_0)\rangle$ with $\hat{H}_S = \hat{H}_{0,S} + \hat{H}_{1,S}$,

and, as for the operators,

$$\hat{A}_I(t) = \exp\left(\frac{i}{\hbar}\hat{H}_{0,S}(t-t_0)\right)\hat{A}_S \exp\left(-\frac{i}{\hbar}\hat{H}_{0,S}(t-t_0)\right). \tag{10}$$

Hence, the Hamiltonian in the interaction picture can then be written as

$$\hat{H}_{0,I}(t) = \exp\left(\frac{i}{\hbar}\hat{H}_{0,S}(t-t_0)\right)\hat{H}_{0,S} \exp\left(-\frac{i}{\hbar}\hat{H}_{0,S}(t-t_0)\right) \tag{11a}$$

and

$$\hat{H}_{1,I}(t) = \exp\left(\frac{i}{\hbar}\hat{H}_{0,S}(t-t_0)\right)\hat{H}_{1,S} \exp\left(-\frac{i}{\hbar}\hat{H}_{0,S}(t-t_0)\right). \tag{11b}$$

It is more convenient to take $\hat{H}_{0,S}$ to be the time independent, for example $\hat{H}_{0,S}$ can be the atomic Hamiltonian. In this case, $\hat{H}_{1,S}$ governs the time dependence of the quantum states of the system according to Schrödinger's equation. Now, let's look at Schrödinger's equation in the interaction picture:

$$\begin{aligned} i\hbar\frac{\partial}{\partial t}|\Psi_I(t)\rangle &= i\hbar\frac{d}{dt}\exp\left(\frac{i}{\hbar}\hat{H}_{0,S}(t-t_0)\right)|\Psi_S(t)\rangle \\ &= -\hat{H}_{0,S}|\Psi_I(t)\rangle + \exp\left(\frac{i}{\hbar}\hat{H}_{0,S}(t-t_0)\right)i\hbar\frac{\partial}{\partial t}|\Psi_S(t)\rangle \\ &= -\hat{H}_{0,S}|\Psi_I(t)\rangle + \exp\left(\frac{i}{\hbar}\hat{H}_{0,S}(t-t_0)\right)\left(\hat{H}_{0,S}\right. \\ &\qquad \left. + \hat{H}_{1,S}(t)\right)|\Psi_S(t)\rangle \\ &= \hat{H}_{1,I}(t)|\Psi_I(t)\rangle. \end{aligned} \tag{12}$$

Eq. 12 is particularly very useful in the formulation of the time dependent perturbation theory. If we try to get Schrödinger's equation in the interaction picture in terms of the time evolution operator $\hat{U}_I$, one can write

$$|\Psi_I(t)\rangle = \hat{U}_I(t,t_0)|\Psi_I(t_0)\rangle. \tag{13}$$

Substituting Eq.13 in Eq.12, we get

$$i\hbar\frac{d}{dt}\hat{U}_I(t,t_0) = \hat{H}_{1,I}(t)\hat{U}_I(t,t_0). \tag{14}$$

Now, let's rewrite the Hamiltonian in the interaction picture with the introduction of a dimensionless parameter λ as

$$\hat{H}_I = \hat{H}_{0,I} + \lambda\,\hat{H}_{1,I}(t). \tag{15}$$

The time evolution operator can be written as

$$\hat{U}_I(t,t_0) = \hat{U}_I^0(t,t_0) + \lambda\hat{U}_I^1(t,t_0) + \lambda^2\hat{U}_I^2(t,t_0) + \cdots \tag{16}$$

where $\hat{U}_I^n$ is the n^{th} correction to the time evolution operator in the interaction picture. If we substitute Eq.16 in Eq.14, we get

$$i\hbar\frac{d}{dt}\hat{U}_I^0(t,t_0) + i\hbar\lambda\frac{d}{dt}\hat{U}_I^1(t,t_0) + i\hbar\lambda^2\frac{d}{dt}\hat{U}_I^2(t,t_0) + i\hbar\lambda^3\frac{d}{dt}\hat{U}_I^3(t,t_0) + \cdots = \tag{17}$$

$$\lambda\hat{H}_{1,I}(t)\hat{U}_I^0(t,t_0) + \lambda^2\hat{H}_{1,I}^1(t)\hat{U}_I^1(t,t_0) + \lambda^3\hat{H}_{1,I}(t)\hat{U}_I^2(t,t_0) + \cdots.$$

By matching the orders of λ on both sides, we get

$$i\hbar\frac{d}{dt}\hat{U}_I^0(t,t_0) = 0 \tag{18a}$$

$$i\hbar\frac{d}{dt}\hat{U}_I^1(t,t_0) = \hat{H}_{1,I}(t)\hat{U}_I^0(t,t_0) \tag{18b}$$

$$i\hbar\frac{d}{dt}\hat{U}_I^2(t,t_0) = \hat{H}_{1,I}(t)\hat{U}_I^1(t,t_0) \tag{18c}$$

$$\vdots$$

$$i\hbar\frac{d}{dt}\hat{U}_I^{n+1}(t,t_0) = \hat{H}_{1,I}(t)\hat{U}_I^n(t,t_0). \tag{18d}$$

Solving Eq.18a gives

$$\hat{U}_I^0(t,t_0) = const = \hat{I}. \tag{19}$$

Rest of the equations in Eq.18 give

$$\hat{U}_I^1(t,t_0) = \hat{I} - \frac{i}{\hbar}\int_{t_0}^{t} dt_1\hat{H}_{1,I}(t_1)\underbrace{\hat{U}_I^0(t_1,t_0)}_{\hat{I}} \tag{19a}$$

$$\begin{aligned}\hat{U}_I^2(t,t_0) &= \hat{I} - \frac{i}{\hbar}\int_{t_0}^{t} dt_2\hat{H}_{1,I}(t_2)\hat{U}_I^1(t_2,t_0) \\ &= \hat{I} + \left(-\frac{i}{\hbar}\right)\int_{t_0}^{t} dt_2\hat{H}_{1,I}(t_2) + \left(-\frac{i}{\hbar}\right)^2\int_{t_0}^{t} dt_2\int_{t_0}^{t_2} dt_1\hat{H}_{1,I}(t_2)\hat{H}_{1,I}(t_1)\end{aligned} \tag{19b}$$

$$\begin{aligned}\hat{U}_I^3(t,0) &= \hat{I} - \frac{i}{\hbar}\int_{t_0}^{t} dt_3\hat{H}_{1,I}(t_3)\hat{U}_I^2(t_3,t_0) \\ &= \hat{I} - \frac{i}{\hbar}\int_{t_0}^{t} dt_3\hat{H}_{1,I}(t_3) \\ &+ \left(-\frac{i}{\hbar}\right)^2\int_{t_0}^{t} dt_3\int_{t_0}^{t_3} dt_2\hat{H}_{1,I}(t_3)\hat{H}_{1,I}(t_2) \\ &+ \left(-\frac{i}{\hbar}\right)^3\int_{t_0}^{t} dt_3\int_{t_0}^{t_3} dt_2\int_{t_0}^{t_2} dt_1\hat{H}_{1,I}(t_3)\hat{H}_{1,I}(t_2)\hat{H}_{1,I}(t_1)\ .\end{aligned} \tag{19c}$$

If we generalize this, we get

$$\begin{aligned}&\hat{U}_I(t,t_0) \\ &= \hat{I} + \sum_{n=1}^{\infty}\left(-\frac{i}{\hbar}\right)^n\int_{t_0}^{t} dt_n\int_{t_0}^{t_n} dt_{n-1}\int_{t_0}^{t_{n-1}} dt_{n-2}\ldots\int_{t_0}^{t_2} dt_1\hat{H}_{1,I}(t_n)\hat{H}_{1,I}(t_{n-1})\ldots\hat{H}_{1,I}(t_1)\ .\end{aligned} \tag{20}$$

Here, it should be noted that $t > t_n > t_{n-1} > t_{n-2} > \cdots > t_2 > t_1 > t_0$. This equation is known as Dyson series. To understand how this changes the amplitudes and evolves the phase, let's consider an initial state $|i_S^0\rangle$, which is an eigenstate of the Hamiltonian $\hat{H}_{0,S}$, and a final state $|f_S^0\rangle$, which is also an eigenstate of the Hamiltonian $\hat{H}_{0,S}$. The probability amplitude that state $|i_S^0\rangle$ transition to

state $\left|f_S^0\right\rangle$ after a time t due to the interaction is

$$A(i \to f;t) = \left\langle f_S^0 \left| \exp\left(\frac{i}{\hbar}\hat{H}_{0,S}(t-t_0)\right)\hat{H}_{1,S}(t)\exp\left(-\frac{i}{\hbar}\hat{H}_{0,S}(t)(t-t_0)\right)\right| i_S^0 \right\rangle \tag{21}$$

$$= \exp\left(\frac{i}{\hbar}(E_f - E_i)(t-t_0)\right)\langle f_S^0|\hat{H}_{1,S}|i_S^0\rangle.$$

Now, let's look at the Dyson series again, the total amplitude is

$$A(i \to f;t) = \sum_{n=1}^{\infty} A^n(i \to f;t) \tag{22}$$

with

$$A^0(i \to f;t) = \langle f_S^0|i_S^0\rangle \tag{23}$$

and

$$A^n(i \to f;t) \tag{24}$$

$$= \left\langle f_S^0 \left| \left(-\frac{i}{\hbar}\right)^n \int_{t_0}^{t} dt_n \int_{t_0}^{t_n} dt_{n-1} \int_{t_0}^{t_{n-1}} dt_{n-2} \dots \int_{t_0}^{t_2} dt_1 \hat{H}_{1,I}(t_n)\hat{H}_{1,I}(t_{n-1}) \dots \hat{H}_{1,I}(t_1) \right| i_S^0 \right\rangle$$

$$= \left(-\frac{i}{\hbar}\right)^n \int_{t_0}^{t} dt_n \int_{t_0}^{t_n} dt_{n-1} \int_{t_0}^{t_{n-1}} dt_{n-2} \dots \int_{t_0}^{t_2} dt_1 \langle f_S^0|\hat{H}_{1,I}(t_n)\hat{H}_{1,I}(t_{n-1}) \dots \hat{H}_{1,I}(t_1)|i_S^0\rangle.$$

Expressing Eq.24 in terms of $\hat{H}_{1,S}(t)$ gives

$$A^n(i \to f;t) \tag{25}$$

$$= \left\langle f_S^0 \left| \left(-\frac{i}{\hbar}\right)^n \int_{t_0}^{t} dt_n \int_{t_0}^{t_n} dt_{n-1} \int_{t_0}^{t_{n-1}} dt_{n-2} \dots \int_{t_0}^{t_2} dt_1 \hat{H}_{1,I}(t_n)\hat{H}_{1,I}(t_{n-1}) \dots \hat{H}_{1,I}(t_1) \right| i_S^0 \right\rangle.$$

$$= \left(-\frac{i}{\hbar}\right)^n \int_{t_0}^{t} dt_n \int_{t_0}^{t_n} dt_{n-1} \int_{t_0}^{t_{n-1}} dt_{n-2} \dots \int_{t_0}^{t_2} dt_1 \times$$

$$\langle f_S^0| \exp\left(\frac{i}{\hbar}\hat{H}_{0,S}(t_n - t_0)\right)\hat{H}_{1,S}(t_n)\exp\left(-\frac{i}{\hbar}\hat{H}_{0,S}(t_n - t_0)\right) \times$$

$$\exp\left(\frac{i}{\hbar}\hat{H}_{0,S}(t_{n-1} - t_0)\right)\hat{H}_{1,S}(t_{n-1})\exp\left(-\frac{i}{\hbar}\hat{H}_{0,S}(t_{n-1} - t_0)\right) \times \dots \times$$

$$\exp\left(\frac{i}{\hbar}\hat{H}_{0,S}(t_1 - t_0)\right)\hat{H}_{1,S}(t_1)\exp\left(-\frac{i}{\hbar}\hat{H}_{0,S}(t_1 - t_0)\right)|i_S^0\rangle.$$

Using the closure relation, the integrand in Eq.25 can be written as

$$\exp\left(\frac{i}{\hbar}(E_f - E_n)(t-t_0)\right)\sum_{k_n^0}\langle f_S^0|\hat{H}_{1,S}(t_n)|k_n^0\rangle \times \tag{26}$$

$$\exp\left(\frac{i}{\hbar}(E_n - E_{n-1})(t_n - t_0)\right)\sum_{k_{n-1}^0}\langle k_n^0|\hat{H}_{1,S}(t_{n-1})|k_{n-1}^0\rangle \times \dots \times$$

$$\exp\left(\frac{i}{\hbar}(E_1 - E_i)(t_1 - t_0)\right)\sum_{k_1^0}\langle k_1^0|\hat{H}_{1,S}(t_1)|i_S^0\rangle,$$

where $|k_n^0\rangle$, $|k_{n-1}^0\rangle, \dots, |k_1^0\rangle$ are also the eigenstates of the Hamiltonian $\hat{H}_{0,S}$. Rewriting the probability amplitude in Eq.25 by the virtue of Eq. 26 gives

$$A^n(i \to f;t) = \left(-\frac{i}{\hbar}\right)^n \int_{t_0}^{t} dt_n \int_{t_0}^{t_n} dt_{n-1} \int_{t_0}^{t_{n-1}} dt_{n-2} \dots \int_{t_0}^{t_2} dt_1 \sum_{k_n^0} \sum_{k_{n-1}^0} \dots \sum_{k_1^0} \times \tag{27}$$

$$\exp\left(\frac{i}{\hbar}(E_f - E_{k_n})(t_n - t_0)\right) \langle f_S^0 | \hat{H}_{1,S}(t_n) | k_n^0 \rangle \times$$

$$\exp\left(\frac{i}{\hbar}(E_n - E_{k_{n-1}})(t_{n-1} - t_0)\right) \langle k_n^0 | \hat{H}_{1,S}(t_{n-1}) | k_{n-1}^0 \rangle \times \dots \times$$

$$\exp\left(\frac{i}{\hbar}(E_{k_1} - E_i)(t_1 - t_0)\right) \langle k_1^0 | \hat{H}_{1,S}(t_1) | i_S^0 \rangle.$$

Here, we represent the amplitude diagrammatically,

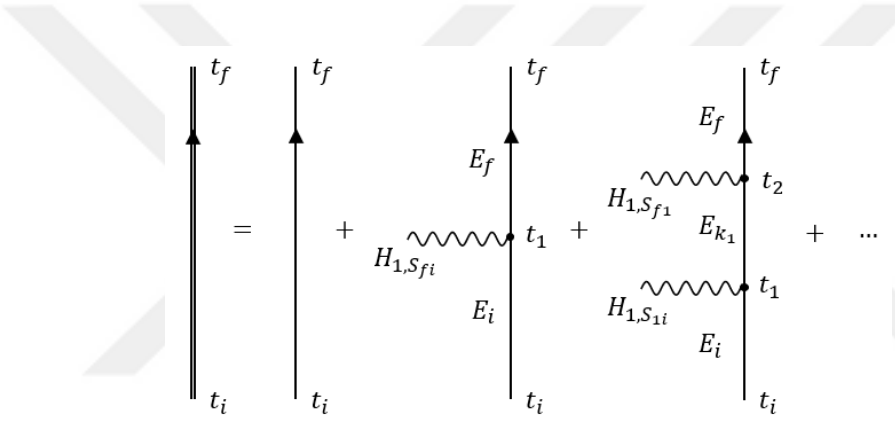


Figure 1: *Diagrammatic representation of the probability amplitude of Dyson series for a transition from* $|i_S^0\rangle$ *at* $t = t_i$ *to* $|f_S^0\rangle$ $t = t_f$. *The matrix element* $\langle i_S^0 | \hat{H}_{1,S}(t) | f_S^0 \rangle$ *is shown as* $H_{1,S_{ij}}$.

Now, let's go back to Eq.20 and define an operator which orders the time as

$$\hat{T}\left[\hat{H}_{1,I}(t_a)\hat{H}_{1,I}(t_b)\right] = \begin{cases} \hat{H}_{1,I}(t_a)\hat{H}_{1,I}(t_b) & if\ t_a > t_b \\ \hat{H}_{1,I}(t_b)\hat{H}_{1,I}(t_a) & if\ t_a < t_b \end{cases}. \tag{28}$$

This *time-ordering operator* allows the integrals to be carried out from 0 to t. Hence Eq.20 becomes

$$\hat{U}_I(t, t_0) \tag{29}$$
$$= \hat{I}$$
$$+ \sum_{n=1}^{\infty} \frac{1}{n!} \left(-\frac{i}{\hbar}\right)^n \int_{t_0}^{t} dt_n \int_{t_0}^{t} dt_{n-1} \int_{t_0}^{t} dt_{n-2} \dots \int_{t_0}^{t} dt_1 \hat{T}\{\hat{H}_{1,I}(t_n)\hat{H}_{1,I}(t_{n-1}) \dots \hat{H}_{1,I}(t_1)\}.$$

Eq.29 can be written in a closed form as

$$\hat{U}_I(t, t_0) = \hat{T} \exp\left(-\frac{i}{\hbar} \int_{t_0}^{t} \hat{H}_{1,I}(t) dt\right). \tag{30}$$

The practical use of Eq.30 in simulations is the consecutive application of Eq.30 in the form of Padé

approximant [35] on a uniform temporal grid with grid spacing δt. The $[1/1]_{\hat{U}_I}$ Padé approximant at about $t = 0$ with temporal grid spacing δt is

$$[1/1]_{\hat{U}_I} = \frac{1 - i\hat{H}_{1,I}\delta t/2}{1 + i\hat{H}_{1,I}\delta t/2} + O(\delta t^3). \tag{31}$$

2.2. Time Dependent Perturbation

In the interaction picture, the Schrödinger's equation given in Eq.12 using the Hamiltonian given in Eq.15 is

$$i\hbar \frac{\partial}{\partial t}|\Psi_I(\vec{r},t)\rangle = \lambda \hat{H}_{1,I}(t)|\Psi(\vec{r},t). \tag{32}$$

If the wave function is expanded in powers of the dimensionless parameter λ, we get

$$|\Psi_I(t)\rangle = \left|\Psi_I^0(t)\right\rangle + \lambda\left|\Psi_I^1(t)\right\rangle + \lambda^2\left|\Psi_I^2(t)\right\rangle + \cdots \tag{33}$$

Substituting Eq.33 in Eq.32 gives

$$\begin{aligned} i\hbar \frac{\partial}{\partial t}\left|\Psi_I^0(t)\right\rangle + i\hbar\lambda \frac{\partial}{\partial t}\left|\Psi_I^1(t)\right\rangle + i\hbar\lambda^2 \frac{\partial}{\partial t}\left|\Psi_I^2(t)\right\rangle + \cdots = \lambda \hat{H}_{1,I}(t)\left|\Psi_I^0(t)\right\rangle \\ + \lambda^2 \hat{H}_{1,I}(t)\left|\Psi_I^1(t)\right\rangle + \lambda^3 \hat{H}_{1,I}(t)\left|\Psi_I^2(t)\right\rangle + \cdots. \end{aligned} \tag{34}$$

Matching the powers of the parameter λ, we have the following set of equations

$$i\hbar \frac{\partial}{\partial t}\left|\Psi_I^0(t)\right\rangle = 0 \tag{35a}$$

$$i\hbar \frac{\partial}{\partial t}\left|\Psi_I^1(t)\right\rangle = \hat{H}_{1,I}(t)\left|\Psi_I^0(t)\right\rangle \tag{35b}$$

$$i\hbar \frac{\partial}{\partial t}\left|\Psi_I^2(t)\right\rangle = \hat{H}_{1,I}(t)\left|\Psi_I^1(t)\right\rangle \tag{35c}$$

$$\vdots$$

$$i\hbar \frac{\partial}{\partial t}\left|\Psi_I^{n+1}(t)\right\rangle = \hat{H}_{1,I}(t)|\Psi_I^n(t)\rangle. \tag{35d}$$

At $t = t_0$, Eq.9 follows

$$|\Psi_I(t_0)\rangle = |\Psi_S(t_0)\rangle. \tag{36}$$

Hence, Eq.33 becomes

$$|\Psi_I(t_0)\rangle = \left|\Psi_I^0(t_0)\right\rangle + \lambda\left|\Psi_I^1(t_0)\right\rangle + \lambda^2\left|\Psi_I^2(t_0)\right\rangle + \cdots = |\Psi_S(t_0)\rangle. \tag{37}$$

Initially, we assume

$$|\Psi_I^n(t_0)\rangle = 0 \qquad (n = 1,2,3 \ldots) \tag{38}$$

Solving Eq.35a gives

$$\left|\Psi_I^0(t)\right\rangle = const = |\Psi_S(t_0)\rangle. \tag{39}$$

Solving Eq.35b with the substitution of Eq.37 gives

$$\left|\Psi_I^1(t)\right\rangle = -\frac{i}{\hbar}\int_{t_0}^{t} dt_1\, \hat{H}_{1,I}(t_1)\, \underbrace{\left|\Psi_I^0(t_1)\right\rangle}_{|\Psi_S(t_0)\rangle}. \tag{40}$$

Similarly, Eq.35c gives

$$\left|\Psi_I^2(t)\right\rangle = -\frac{i}{\hbar}\int_{t_0}^{t} dt_2 \widehat{H}_{1,I}(t_2)\left|\Psi_I^1(t)\right\rangle = \left(-\frac{i}{\hbar}\right)^2 \int_{t_0}^{t} dt_2 \int_{t_0}^{t} dt_1\, \widehat{H}_{1,I}(t_2)\widehat{H}_{1,I}(t_1)|\Psi_S(t_0)\rangle. \tag{41}$$

If we follow the pattern, we can easily generalize the n^{th} order correction as

$$|\Psi_I^n(t)\rangle = \left(-\frac{i}{\hbar}\right)^n \int_{t_0}^{t} dt_n \int_{t_0}^{t_n} dt_{n-1} \dots \int_{t_0}^{t_2} dt_1 \widehat{H}_{1,I}(t_n)\widehat{H}_{1,I}(t_{n-1}) \dots \widehat{H}_{1,I}(t_1)|\Psi_S(t_0)\rangle. \tag{42}$$

One should also be aware here that $t > t_n > t_{n-1} > \cdots > t_2 > t_1 > t_0$. By setting the dimensionless parameter λ to 1 and by the virtue of Eq.33, Eq.26 can be written in Schrödinger's picture as

$$|\Psi_S(t)\rangle = \exp\left(-\frac{i}{\hbar}\widehat{H}_{0,S}(t-t_0)\right)\left\{\underbrace{|\Psi_S(t_0)\rangle}_{initial\ state} + \left|\Psi_I^1(t)\right\rangle + \left|\Psi_I^2(t)\right\rangle + \cdots\right\} \tag{43}$$

2.3. Green's Function

There are number of cases where it is necessary to solve the inhomogeneous Schrödinger's equation that is subject to certain boundary conditions. One of these cases is the perturbation theory where the inhomogeneous term is the perturbation Hamiltonian, $\widehat{H}_{1,I}$ applied to the $(n-1)^{th}$ corrected state $|\Psi_I^{n-1}(t)\rangle$ as seen in Eq.35. The use of Green's functions enables us to picture the perturbation problem in terms of propagating particle. Now, let's consider an inhomogeneous differential equation satisfying given boundary conditions where the position vectors $\vec{r}$ and $\vec{r}'$ lie on the surface S of domain D [31],

$$[z - L(\vec{r})]G(\vec{r},\vec{r}';z) = \delta(\vec{r}-\vec{r}') \tag{44}$$

where z is a complex variable and $L(\vec{r})$ is a hermitian linear operator which admits a complete orthogonal set of eigenfunctions $\{\phi_n(\vec{r})\}$ and corresponding real eigenvalues $\{\lambda_n\}$ by the virtue of

$$L(\vec{r})\phi_n(\vec{r}) = \lambda_n\phi_n(\vec{r}). \tag{45}$$

The normalized eigenfunctions $\{\phi_n(\vec{r})\}$ satisfy the completeness relation

$$\sum_n \phi_n(\vec{r})\phi_n^*(\vec{r}') = \delta(\vec{r}-\vec{r}'), \tag{46}$$

where δ is the Dirac Delta function. If we define

$$(z-L)G(z) = 1 \tag{47}$$

in an abstract vector space, we can show that, in $\vec{r}$-representation, this is indeed Eq.44. To show that let's first express the left-hand side of Eq.47 in $\vec{r}$-representation

$$\langle\vec{r}|(z-L)G(z)|\vec{r}'\rangle = z\langle\vec{r}|\vec{r}'\rangle - \langle\vec{r}|LG(z)|\vec{r}'\rangle \tag{48}$$

using the definitions,

$$\langle \vec{r}|\vec{r}'\rangle = \delta(\vec{r}-\vec{r}') \tag{49}$$

$$\langle \vec{r}|LG(z)\vec{r}'\rangle = L(\vec{r})\langle \vec{r}|G(z)|\vec{r}'\rangle = L(\vec{r})G(\vec{r},\vec{r}';z),$$

we get

$$[z-L(\vec{r})]G(\vec{r},\vec{r}';z). \tag{50}$$

The right-hand side of Eq.47 is simply $\langle \vec{r}|\vec{r}'\rangle$, hence

$$[z-L(\vec{r})]G(\vec{r},\vec{r}';z) = \delta(\vec{r}-\vec{r}'). \tag{51}$$

We should also mention that one can also express Eq.44 in $\vec{k}$-representation by taking the Fourier transform of $G(z)$ and L with respect to position vectors $\vec{r}$ and $\vec{r}'$, giving $L(\vec{k})$ and $G(\vec{k},\vec{k}';z)$, respectively.

In the case of $z \neq \lambda_n$ for all eigenvalues, under the virtue of Eq.45, one can write Eq.47 as

$$G(z) = \frac{1}{z-L}. \tag{52}$$

Multiplying both sides by completeness relation, we obtain

$$G(z) = \frac{1}{z-L}\sum_n |\phi_n\rangle\langle\phi_n| = \sum_n \frac{|\phi_n\rangle\langle\phi_n|}{z-\lambda_n}. \tag{53}$$

The effect of $\frac{1}{z-L}$ on $|\phi_n\rangle$ can easily be seen if one expands $(z-L)^{-1}$ in Taylor series and then re-express it in closed form.

Eq.53 can be divided into two parts as

$$G(z) = \sum_n{}' \frac{|\phi_n\rangle\langle\phi_n|}{z-\lambda_n} + \int dc\, \frac{|\phi_c\rangle\langle\phi_c|}{z-\lambda_c}. \tag{54}$$

Here, the prime in the first term indicates that the summation is over the discrete states $|\phi_n\rangle$, and the integral is over the continuous states $|\phi_c\rangle$. It may also be helpful to express Eq.54 in $\vec{r}$-representation

$$G(\vec{r},\vec{r}';z) = \sum_n{}' \frac{\phi_n(\vec{r})\phi_n^*(\vec{r}')}{z-\lambda_n} + \int dc\, \frac{\phi_c(\vec{r})\phi_c^*(\vec{r}')}{z-\lambda_c}. \tag{55}$$

Before we proceed further, we need to understand the behavior of the denominator in Eq.54 or 55. If $\mathrm{Im}\{z\} \neq 0$ then the denominator of Eq.54 or 55 does not introduce any singularities since L is a hermitian operator which reveals real eigenvalues λ_n, hence $G(z)$ is an analytical function in the complex z-plane. However, if $\mathrm{Im}\{z\} = 0$, then, on the z-plane whenever $z = \lambda_n$, $G(z)$ exhibits a simple pole. In the case of $z = \lambda$, where L reveals continuous eigenvalues corresponding to continuous eigenstates, the integrand in Eq.54 or 55 causes $G(z)$ to misbehave on the real z-axis. To overcome this problem, we need to define $G(z)$ by a limiting procedure. Assuming that the eigenstates are not decaying as $r \to \infty$, one can approach the real z-axis from +imaginary z-axis

given by $G(z=\lambda+i\eta)$ and from $-$imaginary z-axis given by $G(z=\lambda-i\eta)$ for $\eta\to 0^+$. The limit $\eta\to 0^+$ exists, but their values are different across real z-axis. This defines a branch cut in $G(z)$ on complex z-plane. Now, let's define $G(\lambda\pm i\eta)$ in $\vec{r}$-representation

$$G^+(\vec{r},\vec{r}';\lambda)=\lim_{\eta\to 0^+} G(\vec{r},\vec{r}';\lambda+i\eta) \tag{56}$$
$$G^-(\vec{r},\vec{r}';\lambda)=\lim_{\eta\to 0^+} G(\vec{r},\vec{r}';\lambda-i\eta).$$

For an inhomogeneous differential equation, under the virtue of Eq.44,

$$[z-L(\vec{r})]u(\vec{r})=f(\vec{r}), \tag{57}$$

the solution $u(\vec{r})$ can easily be obtained provided that Green's function $G(\vec{r},\vec{r}';z)$ is known. We can easily show that the solution

$$u(\vec{r})=\begin{cases}\int G(\vec{r},\vec{r}';z)f(\vec{r}')d\vec{r}' & z\neq\{\lambda_n\}\\ \int G^{\pm}(\vec{r},\vec{r}';\lambda)f(\vec{r}')d\vec{r}'+u_h(\vec{r}) & z=\lambda\end{cases}, \tag{58}$$

where z is on the branch cut and $u_h(\vec{r})$ is the general solution to $[z-L(\vec{r})]u(\vec{r})=0$, is indeed satisfies Eq.57.

Now let's look at Green's functions' use in quantum mechanics in energy domain ($z=E$) for $\hat{H}_S=\hat{H}_{0,S}+\hat{H}_{1,S}$, where we assume $\hat{H}_{1,S}$ is time-independent perturbation,. From Eq.52, we have

$$G_0(E)=\frac{1}{E-\hat{H}_{0,S}} \tag{59a}$$

and

$$G(E)=\frac{1}{E-\hat{H}_S}=\frac{1}{E-\hat{H}_{0,S}-\hat{H}_{1,S}}. \tag{59b}$$

If we expand Eq.59b, we get

$$G(E)=\frac{1}{E-\hat{H}_{0,S}-\hat{H}_{1,S}}=\frac{1}{E-\hat{H}_{0,S}}+\frac{1}{E-\hat{H}_{0,S}}\hat{H}_{1,S}\frac{1}{E-\hat{H}_{0,S}}+\cdots \tag{60}$$
$$+\frac{1}{E-\hat{H}_{0,S}}\hat{H}_{1,S}\frac{1}{E-\hat{H}_{0,S}}\hat{H}_{1,S}\frac{1}{E-\hat{H}_{0,S}}+\cdots.$$

This can be written as

$$G(E)=G_0(E)\left(1+\hat{H}_{1,S}G_0(E)+\hat{H}_{1,S}G_0(E)\hat{H}_{1,S}G_0(E)+\cdots\right) \tag{61}$$

Eq.61 can be rewritten in closed form as

$$G(E)=G_0(E)+G_0(E)\hat{H}_{1,S}G(E). \tag{62}$$

If Eq.62 is used recursively, it is easily seen that Eq.61 can be obtained. In the $\vec{r}$-representation, by the virtue of the closure relations for $|\vec{r}_1\rangle$ and $|\vec{r}_2\rangle$, Eq.62 becomes

$$G(\vec{r},\vec{r}';E)=G_0(\vec{r},\vec{r}';E)+\int d\vec{r}_1\int d\vec{r}_2\, G_0(\vec{r},\vec{r}_1;E)\hat{H}_{1,S}(\vec{r}_1)\delta(\vec{r}_1-\vec{r}_2)G(\vec{r}_2,\vec{r}';E) \tag{63a}$$

Hence,

$$G(\vec{r},\vec{r}';E) = G_0(\vec{r},\vec{r}';E) + \int d\vec{r}_1 G_0(\vec{r},\vec{r}_1;E)\hat{H}_{1,S}(\vec{r}_1)G(\vec{r}_1,\vec{r}';E). \tag{63b}$$

If $\hat{H}_{1,S}$ is time dependent,

$$G(\vec{r},t;\vec{r}',t';E) = G_0(\vec{r},t;\vec{r}',t';E) + \int d\vec{1}\, G_0(\vec{r},t;\vec{1},E)\hat{H}_{1,S}(\vec{1})G(\vec{1},\vec{r}';E) \tag{64}$$

where $\vec{1}$ stands for the pair ($\vec{r}_1$,t_1). This is Dyson's equation in terms of Green's functions. We must also be careful about the time-ordering as we have discussed it in section: *Time Evolution.*

Given Eq.5, it is easy to find the wave function at a later time t and position $\vec{r}$ as

$$\psi(\vec{r},t) = \langle\vec{r}|\Psi(t)\rangle. \tag{65}$$

Using the closure relation again,

$$\psi(\vec{r},t) = \int d\vec{r}'\langle\vec{r}|\hat{U}\,(t,t')|\vec{r}'\rangle\langle\vec{r}'|\Psi(t')\rangle = \int d\vec{r}'\langle\vec{r}|\hat{U}(t,t')|\vec{r}'\rangle\psi(\vec{r}',t'). \tag{66}$$

More, we want $t > t'$. We do not want propagation backward in time. To prevent that we introduce the Heaviside function θ as

$$\theta(t-t') = \begin{cases} 1 & if\ t > t' \\ 0 & if\ t < t' \end{cases}. \tag{67}$$

With Eq.67, we can now define the *retarded* Green's function propagator as

$$G(\vec{r},t;\vec{r}',t';E) = -\frac{i}{\hbar}\,\theta(t-t')\langle\vec{r}'|\hat{U}(t,t')|\vec{r}\rangle. \tag{68}$$

It is quite easy to see that Eq.68 is indeed the pulse solution of the time-dependent Schrödinger's equation of the form

$$\left[i\hbar\frac{\partial}{\partial t'} - \hat{H}(\vec{r}')\right]\psi_n(\vec{r}')\exp\left(-\frac{i}{\hbar}E_n t'\right) = 0, \tag{69}$$

where $\psi_n(\vec{r})$ are the eigenstates and E_n are the eigenvalues of the Hamiltonian $\hat{H}(\vec{r})$. Rewriting Eq.68 for this Hamiltonian,

$$G(\vec{r},t;\vec{r}',t';E) = -\frac{i}{\hbar}\theta(t-t')\langle\vec{r}'|\exp\left(-\frac{i}{\hbar}\hat{H}(t-t')\right)|\vec{r}\rangle. \tag{70}$$

Using completeness relation, we get

$$\begin{aligned} &G(\vec{r},t;\vec{r}',t';E_n) \\ &= -\frac{i}{\hbar}\theta(t-t')\sum_n\sum_{n'}\langle\vec{r}'\,|\psi_{n'}\rangle\left\langle\psi_{n'}\left|\exp\left(-\frac{i}{\hbar}\,\hat{H}(t-t')\right)\right|\psi_n\right\rangle\langle\psi_n|\vec{r}\rangle \\ &= -\frac{i}{\hbar}\theta(t-t')\sum_n\psi_n^*(\vec{r})\,\psi_n(\vec{r}')\exp\left(-\frac{i}{\hbar}E_n(t-t')\right). \end{aligned} \tag{71}$$

Substituting Eq.71 in Eq.69 gives

$$\left[i\hbar\frac{\partial}{\partial t'} - \hat{H}(\vec{r}')\right]G(\vec{r},t,\vec{r}',t';E_n) = \delta(t'-t)\sum_n\psi_n^*(\vec{r})\psi_n(\vec{r}')\exp\left(-\frac{i}{\hbar}E_n(t-t')\right). \tag{72}$$

Due to Dirac Delta function for $t \neq t'$, right-hand side of Eq.72 is zero. In this case, the right-hand side can be rewritten as

$$\delta(t'-t)\underbrace{\sum_{n}\psi_n^*(\vec{r})\psi_n(\vec{r}')}_{\delta(\vec{r}-\vec{r}')}. \tag{73}$$

Hence,

$$\left[i\hbar\frac{\partial}{\partial t'}-\hat{H}(\vec{r}')\right]G(\vec{r},t,\vec{r}',t';E_n)=\delta(t'-t)\delta(\vec{r}-\vec{r}'). \tag{74}$$

Green's functions in perturbation theory are the propagators. One must always be careful when one deals with time dependent Hamiltonian due to its non-zero commutations with itself at different times.

2.4. Simulation

In this study, we apply the n^{th}order time dependent perturbation theory to High-Order Harmonic Generation (HHG) problem to extract the vital information from the wave function for some special cases. Although, we are interested in HHG from confined systems, where time dependent perturbation theory is important, we focus our attention on the formulation of n^{th} order time dependent perturbation theory using Green's functions method for HHG simulations and its parallelization opportunities. The interaction of the laser field with the target is at the heart of HHG. The target in this study is chosen as the hydrogen atom. The Hamiltonian of the system consists of two parts: The first part is the Hamiltonian of the hydrogen atom which is time independent and designated by $\hat{H}_{a,S}$ in Schrödinger's picture, and the second part is the interaction of the atom with the time dependent laser field which is designated by $\hat{H}_{Int,S}(t)$. The total Hamiltonian $\hat{H}_S(t)$ is then

$$\hat{H}_S(t)=\hat{H}_{a,S}+\hat{H}_{Int,S}(t). \tag{75}$$

The first step in the simulation is to obtain the energy eigenvalue E of the initial state $|\Psi_S(t_0)\rangle$. This can simply be achieved by solving the eigenvalue-eigenfunction problem

$$\hat{H}_{a,S}|\Psi_S(t_0)\rangle=E|\Psi_S(t_0)\rangle. \tag{76}$$

Let's express the radial part of atomic Hamiltonian in $\vec{r}$-representation,

$$\hat{H}_{a,S}R(r)=\left(-\frac{1}{2r}\frac{d^2}{dr^2}r+\frac{l(l+1)}{2r^2}-\frac{1}{r}\right)R(r)=ER(r), \tag{77}$$

where l is the quantum angular momentum number. We should also note that in the writing of Eq.77, atomic units are used. In order to solve this differential equation numerically, we need to express it on a spatial grid with proper boundary conditions. In this study, we employed uniform spatial grid consists of $N+1$ points starting from $r_0=0$ to $r_N=r_f$ with grid spacing δr. The conventional boundary conditions are that the radial part of the wave function vanishes at $r=0$ and at $r\to\infty$. Numerically, we choose r_f large enough to compensate for $r\to\infty$. Now, to express the atomic

Hamiltonian in matrix form on this discrete spatial grid, we adapt the central derivative formula

$$U'' = \frac{U_{i+1} - 2U_i + U_{i-1}}{\delta r^2} + O(\delta r^2), \tag{78}$$

where $U_i = r_i R(r_i)$ and $r_i = i\delta r$. Eq.77 can be written in terms of U as

$$-\frac{1}{2}\frac{d^2U}{dr^2} + \frac{l(l+1)}{2r^2}U - \frac{U}{r} = EU. \tag{79}$$

Discretizing Eq.79 by the virtue of Eq.78 gives

$$-\frac{1}{2\delta r^2}(U_{i+1} - 2U_i + U_{i-1}) + \frac{l(l+1)}{2r^2}U_i - \frac{U_i}{r_i} = EU_i. \tag{80}$$

If Eq.80 is written for each i starting from 0 to N with the boundary conditions $U_0 = 0$ and $U_N = 0$, we get the following matrix equation

$$\begin{bmatrix} \beta_1 & \alpha & 0 & 0 & \cdots & 0 & 0 & 0 \\ \alpha & \beta_2 & \alpha & 0 & \cdots & 0 & 0 & 0 \\ 0 & \alpha & \beta_3 & \alpha & \cdots & 0 & 0 & 0 \\ 0 & 0 & \alpha & \beta_4 & \cdots & 0 & 0 & 0 \\ 0 & 0 & 0 & 0 & \cdots & 0 & 0 & 0 \\ \vdots & \vdots & \vdots & \vdots & \cdots & \vdots & \vdots & \vdots \\ 0 & 0 & 0 & 0 & \cdots & \alpha & \beta_{N-2} & \alpha \\ 0 & 0 & 0 & 0 & \cdots & 0 & \alpha & \beta_{N-1} \end{bmatrix} \begin{bmatrix} U_1 \\ U_2 \\ U_3 \\ U_4 \\ \vdots \\ U_{N-3} \\ U_{N-2} \\ U_{N-1} \end{bmatrix} = E \begin{bmatrix} U_1 \\ U_2 \\ U_3 \\ U_4 \\ \vdots \\ U_{N-3} \\ U_{N-2} \\ U_{N-1} \end{bmatrix}, \tag{81}$$

where

$$\beta_i = \frac{1}{\delta r^2} + \frac{l(l+1)}{2r_i} - \frac{1}{r_i} \tag{82}$$

$$\alpha = -\frac{1}{2\delta r^2}.$$

The eigenvalues of the coefficient matrix given in Eq.81 can easily be found by means of LAPACK [36] routines. Once we calculate the energy eigenvalue of state we are interested in, it is time to find the corresponding eigenstate: There are several ways to achieve this. One of methods is called the *relaxation method*. Initially a trial wave function is selected and iteratively relaxed to the ground state. Provided that the trial wave function is close to the ground state wave function, the convergence is very fast. However, this method works only for the ground-state energy. In order to find the n^{th} excited state wave function, it is necessary to find the first $n-1$ excited state wave functions and project them out as we go up. Another method is called the *shooting method*. This is the method we employ in our simulations. It is easy to implement as long as we know the energy eigenvalue of the desired state. This method allows us to calculate the desired excited state directly without the need to find the lower excited states up to that one. This method, however, may have issues if confined potential is introduced. In the formal formalism, the spatial domain is divided into two regions separated by the classical turning point. Then one starts shooting from one end satisfying the boundary condition on that end with a guess for the next point. Simultaneously, one starts to shoot from the other end satisfying the boundary condition on that end, again, with a guess for the next point. These two points merge at the classical turning point and then the wave function is

normalized. In the case of confinement, one should be careful about multiple classical turning points. It is always a good practice to apply the Hamiltonian to the normalized wave function to see if we truly found the desired state. A typical convergence threshold in such cases is is at the order of $10^{-13} - 10^{-16}$.

We have already defined the atomic Hamiltonian $\hat{H}_{a,S}$ in Eq.75. Now, let's define the interaction Hamiltonian $\hat{H}_{Int,S}(t)$. We consider a linearly (z-) polarized laser field where the z component of the electric field interacts with the hydrogen atom. We can define the interaction Hamiltonian in length gauge within the dipole approximation as

$$\hat{H}_{Int,S}(t) = rf(t)\cos(\theta). \tag{83}$$

Here, $f(t)$ is the laser profile of the form

$$f(t) = F_0 \exp\left(-4ln2\frac{t^2}{T_{FWHM}^2}\right)\cos(\omega_0 t), \tag{84}$$

where F_0 is peak value of the electric field, ω_0 is the frequency of the driving laser, and T_{FWHM} is the pulse duration at full-width-half-maximum.

Going back to Eq.1 with the Hamiltonian given by Eq.75, the perturbative solution is given by Eq.43. Keeping only the first correction to the wave function, if we substitute Eq.43 in Eq.1, we get, in $\vec{r}$-representation,

$$\left(i\frac{\partial}{\partial t} - \hat{H}_{a,S}\right)\Psi_S^1(\vec{r},t) = \hat{H}_{Int,S}\Psi_S^0(\vec{r})\exp(-iE_0 t) + \hat{H}_{Int,S}(t)\Psi_S^1(\vec{r},t), \tag{85}$$

where $\Psi_S^0(\vec{r}) = \Psi_S(\vec{r})$, the initial wave function, and E_0 is the energy eigenvalue of the initial state. The second term on the right-hand side is small enough so that we can ignore it. We should also mention that the Eq.85 is expressed in atomic units. Hence, Eq.85 becomes

$$\left(i\frac{\partial}{\partial t} - \hat{H}_{a,S}\right)\Psi_S^1(\vec{r},t) = \hat{H}_{Int,S}(t)\Psi_S^0(\vec{r})\exp(-iE_0 t). \tag{86}$$

Feeding the solution of Eq.86 back into itself gives higher order perturbation terms as

$$\begin{aligned}
\left(i\frac{\partial}{\partial t} - \hat{H}_{a,S}\right)\Psi_S^2(\vec{r},t) &= \hat{H}_{Int,S}(t)\Psi_S^1(\vec{r},t) \\
\left(i\frac{\partial}{\partial t} - \hat{H}_{a,S}\right)\Psi_S^3(\vec{r},t) &= \hat{H}_{Int,S}(t)\Psi_S^2(\vec{r},t) \\
&\vdots \\
\left(i\frac{\partial}{\partial t} - \hat{H}_{a,S}\right)\Psi_S^n(\vec{r},t) &= \hat{H}_{Int,S}(t)\Psi_S^{n-1}(\vec{r},t).
\end{aligned} \tag{87}$$

Now let's look at Eq.86 again,

$$\left(i\frac{\partial}{\partial t} - \hat{H}_{a,S}\right)\Psi_S^1(\vec{r},t) = S(\vec{r},t), \tag{88}$$

where the $S(\vec{r},t)$ is the right-hand side of Eq.86. This is inhomogeneous time dependent Schrödinger's equation with the source term $S(\vec{r},t)$. Rewriting Eq.88 and integrating it from $t' = t$

to $t' = t + \delta t$ gives

$$i\int_t^{t+\delta t} \frac{\partial}{\partial t}\Psi_S^1(\vec{r},t')dt' - \int_t^{t+\delta t} \hat{H}_{a,S}\Psi_S^1(\vec{r},t')dt' = \int_t^{t+\delta t} S(\vec{r},t')dt'. \tag{89}$$

Integrating the terms on the left-hand side using trapezoid rule and integrating the term on the right-hand side with rectangle rule, picking the middle temporal point, we get,

$$i\Psi_S^1(\vec{r},t+\delta t) - i\Psi_S^1(\vec{r},t) - \hat{H}_{a,S}\frac{\delta t}{2}\left(\Psi_S^1(\vec{r},t+\delta t) + \Psi_S^1(\vec{r},t)\right) = \delta t S\left(\vec{r},t+\frac{\delta t}{2}\right). \tag{90}$$

Solving for $\Psi_S^1(\vec{r},t+\delta t)$ gives

$$\Psi_S^1(\vec{r},t+\delta t) = \left[\frac{1-i\hat{H}_{a,S}\frac{\delta t}{2}}{1+i\hat{H}_{a,S}\frac{\delta t}{2}}\right]\Psi_S^1(\vec{r},t) - \frac{i\delta t}{1+i\hat{H}_{a,S}\frac{\delta t}{2}} S\left(\vec{r},t+\frac{\delta t}{2}\right) + O(\delta t^3). \tag{91}$$

At this point, we prefer to expand the wave function in the basis of the eigenstates of the angular momentum operator $\hat{L}^2$. This gives us the following partial wave expansion

$$\Psi_S^1(\vec{r},t) = \sum_{l=0}^{\infty}\sum_{m=-l}^{l} u_l^1(\vec{r},t)Y_l^m(\theta,\phi). \tag{92}$$

The intensity is weak enough so that we can ignore the effect of magnetic field here, hence we have the freedom of choosing m. We choose $m = 0$ for simplicity. This will drop down the summation over m. Also, the summation over l goes to infinity, however we will limit ourselves to some maximum value l_{max} due to computational reasons.

In order to solve Eq.91, let's look at each term separately. Let

$$\left[\frac{1-i\hat{H}_{a,S}\frac{\delta t}{2}}{1+i\hat{H}_{a,S}\frac{\delta t}{2}}\right]\Psi_S^1(\vec{r},t) = \sum_{l}^{l_{max}} g_l^1(\vec{r},t)Y_l^0(\theta,\phi) \tag{93}$$

and

$$-\frac{i\delta t}{1+i\hat{H}_{a,S}\frac{\delta t}{2}}\hat{H}_{Int,S}\left(t+\frac{\delta t}{2}\right)u_{l_0}^0 Y_{l_0}^0(\theta,\phi)\exp\left(-iE_0\left(t+\frac{\delta t}{2}\right)\right) = \sum_{l}^{l_{max}} h_l^1\left(\vec{r},t+\frac{\delta t}{2}\right)Y_l^0(\theta,\phi). \tag{94}$$

Here, $u_{l_0}^0$ is the radial part of the initial wave function. For example, if the initial state is $|1s\rangle$ of hydrogen atom, then it is $rR_{n=1,l_0=0}$. g_l^1 and h_l^1 in Eq.93 and Eq.94, respectively, are the radial parts of the intermediates. Discretizing both spatial and temporal dimensions, Eq.92 becomes

$$\Psi_{\mathrm{S,i}}^{1,k} = \sum_{l}^{l_{max}} u_{l,i}^{1,k} Y_l^0(\theta,\phi), \tag{95}$$

where k stands for the k^{th} temporal point, i represents i^{th} spatial point. Similarly, Eq.93 becomes

$$\sum_{l}^{l_{max}} g_{l,i}^{1,k} Y_l^0(\theta,\phi) = \left[\frac{1 - i\widehat{H}_{a,S,i}\frac{\delta t}{2}}{1 + i\widehat{H}_{a,S,i}\frac{\delta t}{2}}\right] \sum_{l}^{l_{max}} u_{l,i}^{1,k} Y_l^0(\theta,\phi) \tag{96}$$

and Eq.94 becomes

$$-\frac{i\delta t}{1 + i\widehat{H}_{a,S,i}\frac{\delta t}{2}} r_i f^{k+\frac{1}{2}} \cos(\theta)\, u_{l_0,i}^0 Y_{l_0}^0 \exp\left(-iE_0\, \delta t\left(k + \frac{1}{2}\right)\right). \tag{97}$$

Multiplying both sides of Eq.96 and Eq.97 by $Y_{l^*}^0$ and integrating over the full solid angle give the following equations for a given l^* with the substitution $l \leftarrow l^*$ as

$$\begin{aligned} -\frac{i\delta t}{4\delta r^2} g_{l,i+1}^{1,k} + \left[1 + \frac{i\delta t}{2}\left(\frac{1}{\delta r^2} - \frac{1}{r_i} + \frac{l(l+1)}{2r_i^2}\right)\right] g_{l,i}^{1,k} - \frac{i\delta t}{4\delta r^2} g_{l,i-1}^{1,k} \\ = \frac{i\delta t}{4\delta r^2} u_{l,i+1}^{1,k} + \left[1 - \frac{i\delta t}{2}\left(\frac{1}{\delta r^2} - \frac{1}{r_i} + \frac{l(l+1)}{2r_i^2}\right)\right] u_{l,i}^{1,k} + \frac{i\delta t}{4\delta r^2} u_{l,i-1}^{1,k}. \end{aligned} \tag{98}$$

$$\begin{aligned} -\frac{i\delta t}{4\delta r^2} h_{l,i+1}^{1,k} + \left[1 + \frac{i\delta t}{2}\left(\frac{1}{\delta r^2} - \frac{1}{r_i} + \frac{l(l+1)}{2r_i^2}\right)\right] h_{l,i}^{1,k} - \frac{i\delta t}{4\delta r^2} h_{l,i-1}^{1,k} \\ = i\delta t r_i f^{k+\frac{1}{2}} u_{l_0}^0 \left(C_{l_{0-1}}\delta_{l_0-1,l} + C_{l_0}\delta_{l_0+1,l}\right) \exp\left(-iE_0 t_{k+\frac{1}{2}}\right), \end{aligned} \tag{99}$$

respectively. Here, $\delta_{m,n}$ is the Kronecker-Delta, and $C_l = \sqrt{\frac{(l+1)^2}{(2l+1)(2l+3)}}$. With the following additional definitions,

$$\begin{aligned} \gamma &= \frac{i\delta t}{2} \\ \Gamma_i &= \frac{1}{\delta r^2} - \frac{1}{r_i} + \frac{l(l+1)}{2r_i^2} \\ \zeta &= \frac{i\delta t}{4\delta r^2}, \end{aligned} \tag{100}$$

we can write Eq.98 and Eq.99 in a matrix form as

$$\begin{bmatrix} 1+\gamma\Gamma_1 & -\zeta & 0 & 0 & \cdots & 0 & 0 \\ -\zeta & 1+\gamma\Gamma_2 & -\zeta & 0 & \cdots & 0 & 0 \\ 0 & -\zeta & 1+\gamma\Gamma_3 & -\zeta & \cdots & 0 & 0 \\ \vdots & \vdots & \vdots & \vdots & \cdots & \vdots & \vdots \\ 0 & 0 & 0 & 0 & \cdots & 1+\gamma\Gamma_{N-2} & -\zeta \\ 0 & 0 & 0 & 0 & \cdots & -\zeta & 1+\gamma\Gamma_{N-1} \end{bmatrix} \begin{bmatrix} g_{l,1}^{1,k} \\ g_{l,2}^{1,k} \\ \vdots \\ g_{l,N-2}^{1,k} \\ g_{l,N-1}^{1,k} \end{bmatrix} \tag{101}$$

$$= \begin{bmatrix} \zeta u_{l,2}^{1,k} + [1-\gamma\Gamma_1] u_{l,1}^{1,k} \\ \zeta u_{l,3}^{1,k} + [1-\gamma\Gamma_2] u_{l,2}^{1,k} + \zeta u_{l,1}^{1,k} \\ \vdots \\ \zeta u_{l,N-1}^{1,k} [1-\gamma\Gamma_{N-2}] u_{l,N-2}^{1,k} + \zeta u_{l,N-3}^{1,k} \\ [1-\gamma\Gamma_{N-1}] u_{l,N-1}^{1,k} + \zeta u_{l,N-2}^{1,k} \end{bmatrix},$$

and

$$\begin{bmatrix} 1+\gamma\Gamma_1 & -\zeta & 0 & 0 & \cdots & 0 & 0 \\ -\zeta & 1+\gamma\Gamma_2 & -\zeta & 0 & \cdots & 0 & 0 \\ 0 & -\zeta & 1+\gamma\Gamma_3 & -\zeta & \cdots & 0 & 0 \\ \vdots & \vdots & \vdots & \vdots & \cdots & \vdots & \vdots \\ 0 & 0 & 0 & 0 & \cdots & 1+\gamma\Gamma_{N-2} & -\zeta \\ 0 & 0 & 0 & 0 & \cdots & -\zeta & 1+\gamma\Gamma_{N-1} \end{bmatrix} \begin{bmatrix} h_{l,1}^{1,k} \\ h_{l,2}^{1,k} \\ \vdots \\ h_{l,N-2}^{1,k} \\ h_{l,N-1}^{1,k} \end{bmatrix} \tag{102}$$

$$= \begin{bmatrix} -i\delta tr_1 f^{k+\frac{1}{2}}\left(C_{l_0-1}\delta_{l_0-1,l} + C_{l_0}\delta_{l_0+1,l}\right)u_{l_0,1}^0 \exp\left(-iE_0 t_{k+\frac{1}{2}}\right) \\ -i\delta tr_2 f^{k+\frac{1}{2}}\left(C_{l_0-1}\delta_{l_0-1,l} + C_{l_0}\delta_{l_0+1,l}\right)u_{l_0,2}^0 \exp\left(-iE_0 t_{k+\frac{1}{2}}\right) \\ \vdots \\ -i\delta tr_{N-2} f^{k+\frac{1}{2}}\left(C_{l_0-1}\delta_{l_0-1,l} + C_{l_0}\delta_{l_0+1,l}\right)u_{l_0,N-2}^0 \exp\left(-iE_0 t_{k+\frac{1}{2}}\right) \\ -i\delta tr_{N-1} f^{k+\frac{1}{2}}\left(C_{l_0-1}\delta_{l_0-1,l} + C_{l_0}\delta_{l_0+1,l}\right)u_{l_0,N-1}^0 \exp\left(-iE_0 t_{k+\frac{1}{2}}\right) \end{bmatrix},$$

respectively. First order correction $u_{l,i}^{1,k}$ at t_k can be obtained by solving the unknowns $g_{l,i}^{1,k}$ in Eq.101 and $h_{l,i}^{1,k}$ in Eq.102. It is not difficult to go higher order corrections with this Green's function method. Once the n^{th} order correction $\Psi_{S,i}^{n,k}$ is obtained, one can calculate the $(n+1)^{th}$ order correction recursively solving Eq.101 and Eq.102. However, for $n \geq 2$, the right-hand side of Eq.102 needs to be changed to

$$\begin{bmatrix} -i\delta tr_1 f^{k+\frac{1}{2}}\left(C_{l-1}u_{l-1,1}^{n-1,k} + C_l u_{l+1,1}^{n-1,k}\right) \\ -i\delta tr_2 f^{k+\frac{1}{2}}\left(C_{l-1}u_{l-1,2}^{n-1,k} + C_l u_{l+1,2}^{n-1,k}\right) \\ \vdots \\ -i\delta tr_{N-2} f^{k+\frac{1}{2}}\left(C_{l-1}u_{l-1,N-2}^{n-1,k} + C_l u_{l+1,N-2}^{n-1,k}\right) \\ -i\delta tr_{N-1} f^{k+\frac{1}{2}}\left(C_{l-1}u_{l-1,N-1}^{n-1,k} + C_l u_{l+1,N-1}^{n-1,k}\right) \end{bmatrix}. \tag{103}$$

2.5. Power Spectrum

The power spectrum can be described in several ways [37]. At every temporal point in the time domain D_T, we calculate the expectation value of the induced dipole $\langle z(t)\rangle$, dipole velocity $\langle \dot{z}(t)\rangle$, and dipole acceleration $\langle \ddot{z}(t)\rangle$ caused by the driving laser. In this study, we used expectation value of the dipole acceleration to generate the power spectrum. The dipole acceleration is calculated as

$$\langle \ddot{z}(t)\rangle = -\left\langle \Psi_S(t) \middle| \left[\left[\hat{z}_S, \hat{H}_S(t)\right], \hat{H}_S(t)\right] \middle| \Psi_S(t) \right\rangle - E(t) \tag{104}$$

where $E(t)$ is the electric field. This represents the contribution from the driving laser, which only strengthens the first harmonic.

The power spectrum is given as

$$P_{\mu}(\omega) \propto \left| \int_{t_0}^{t_f} \exp(-i\omega t)\, \langle \mu(t) \rangle dt \right|^2 , \tag{105}$$

where μ could be either of the following $\langle z \rangle, \langle \dot{z} \rangle$, or $\langle \ddot{z} \rangle$. In our case, $\mu = \langle \ddot{z} \rangle$ and t_f is the final time of the simulation.

2.6. Notes on Parallelization

The matrix equations in Eq.101 and Eq.102 have the dimension $(N-2) \times (N-2)$. Also, it should be noted that these equations need to be solved simultaneously for $l_{lmax} + 1$ times. However, in each equation, l is just a parameter. This is one of the advantages of expressing the wave function $\Psi_S(\vec{r}, t)$ in the basis of $\hat{L}^2$. The orthogonality of the spherical harmonics decouples the matrix equations given above and enables parallelization. One can simply distribute the radial parts in the partial wave expansion associated with each l value corresponding to the same time t on multiple CPU cores or even on GPU. In this study, we only considered the parallelization on CPU cores using OpenMP [38]. OpenMP provides us a parallelization framework with a set of easy-to-use compiler directives. Message-Passing Interface [39,40] may also be used here, but we do not see much prospect for it due to data transfer overhead among distributed compute nodes.

3. RESULTS AND DISCUSSIONS

3.1. Simulation

We developed our own simulation program in C programming language implementing the formalism we derived in the *Theory* chapter. The matrix equations given by Eq.101, 102, and 103 are solved for each angular momentum value l in the partial wave expansion up to the maximum value, l_{max}. Partial list of the control parameters of our program is given in Table 1.

Symbol	Unit	Description
I0	$\frac{W}{cm^2}$	The peak intensity of the driving laser
qn, ql	–	The principal quantum number and the angular quantum number of the initial state. The current implementation only takes an eigenstate of the Hamiltonian $\hat{H}_{a,S}$.
perturborder	–	This is the order of the maximum correction to the wave function.
nthreads	–	Number of CPU threads.
dr	$a.u.$	Spatial grid spacing
tfac	–	This is the number of temporal points per Rydberg period for the given initial state qn, ql.
lmax	–	Number of terms in the partial wave expansion.
w0	$a.u.$	Driving laser frequency, ω_0.
ncycle	–	Total number of cycles of the pulse
ncyclefwhm	–	Number of cycles at FWHM.
rf	$a.u.$	Maximum spatial grid size (the numerical representation of $r \to \infty$ at which $\Psi(\text{rf}) = 0$).

Table 1: *Partial control parameters of our program.*

We carried out convergence tests on the dipole, dipole velocity, and dipole acceleration to determine the value of l_{max} ($lmax$ in control parameters). We also looked at the dependence of l_{max} on the power spectrum. We found that for a free hydrogen atom, the results are practically indistinguishable for $l_{max} \geq 60$. However, we should note that from our previous experience [34], in the confined case (i.e. hydrogen atom confined inside a fullerene), l_{max} needs to be much higher.

We conducted another convergence test on the value of r_f (rf in control parameters) and we found that for a grid of $\mathrm{r_f} = 300$ at $3.0 \times 10^{14}\ W/cm^2$ (I0 in control parameters) is sufficient. We choose a linearly polarized monochromatic laser with $800\ nm$ wavelength ($\mathrm{w0} = 0.057$ in control parameters). The total pulse duration is 16 cycles (ncycles in control parameters) with 4 cycles at FWHM (ncyclefwhm in control parameters).

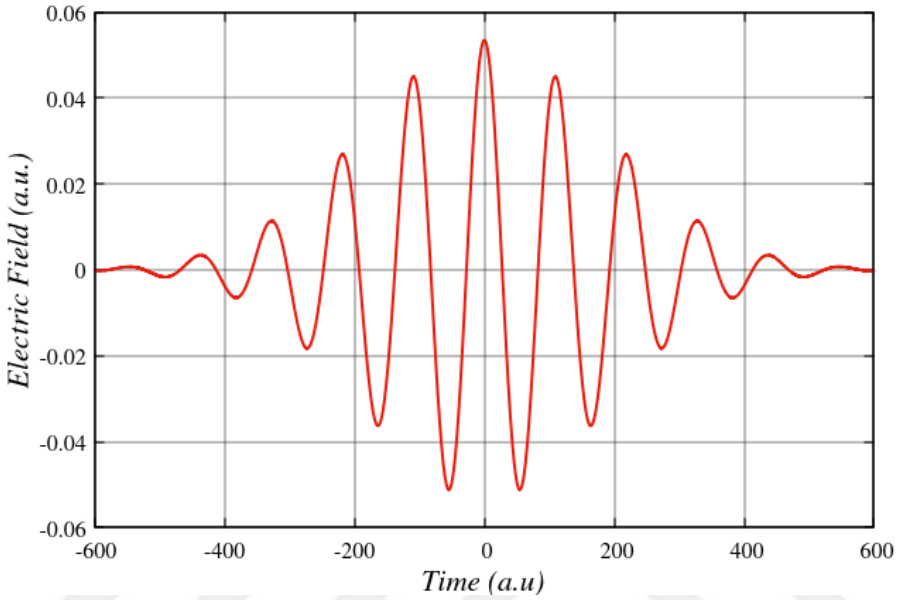


Figure 2: *Driving laser profile. The peak intensity is* $\mathbf{1.0 \times 10^{14}\ \frac{W}{cm^2}}$, *wavelength is* $\mathbf{800\ nm}$.

The initial state used in the following simulations is the hydrogen atom's ground state. We used 0.5 for spatial grid spacing (dr in control parameters) which makes 601 spatial grid points, we used 0.05 for the number of temporal grid points per Rydberg period (6.28 $a.u.$ for the ground state) which makes 5615 temporal points. The spatial grid spacing we used is acceptable for the purpose of this study. However, for other purposes, we advise much denser spatial grid, such as $\mathrm{dr} = 0.01$, to be used in the simulations, which leads to 0.5% fractional error in the energy calculation compared to the ground state energy of the hydrogen atom which is 0.5 Hartree. The fractional error in this current calculation of $\langle \Psi_S(0) | \hat{H}_{a,S} | \Psi_S(0) \rangle$ with respect to the eigenvalue obtained from LAPACK is at the order of 10^{-16}. The fractional error with respect to 0.5 Hartree is 5.6%.

We compare HHG spectrum of various orders of perturbation with that of the TDSE [37]. The TDSE code was developed during earlier work [34,41].

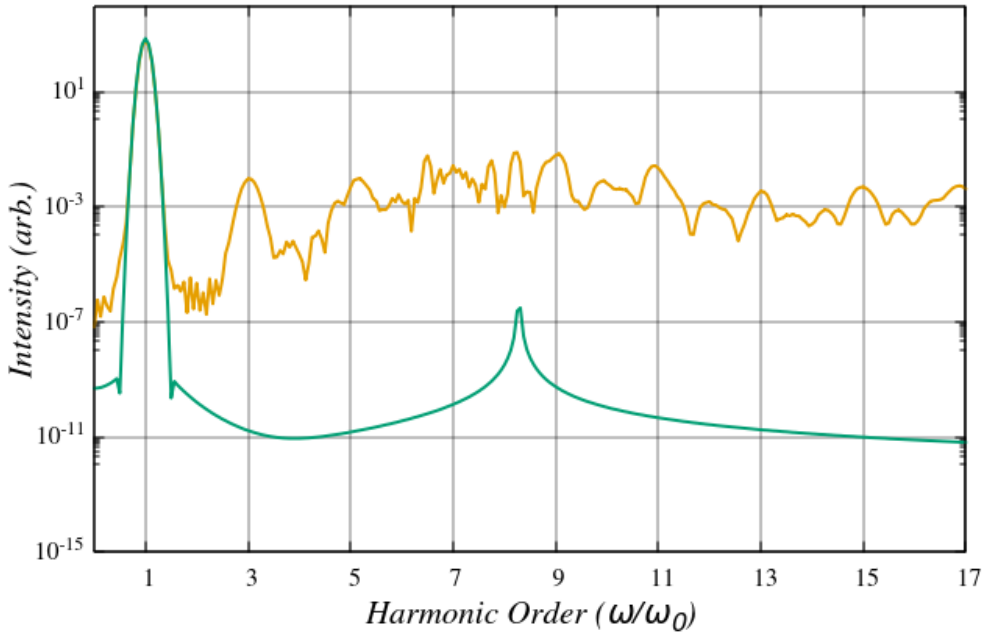


Figure 3: *Comparison of the power spectrum of TDSE (orange curve) with that of the* 1^{st} *order Perturbation (green curve).*

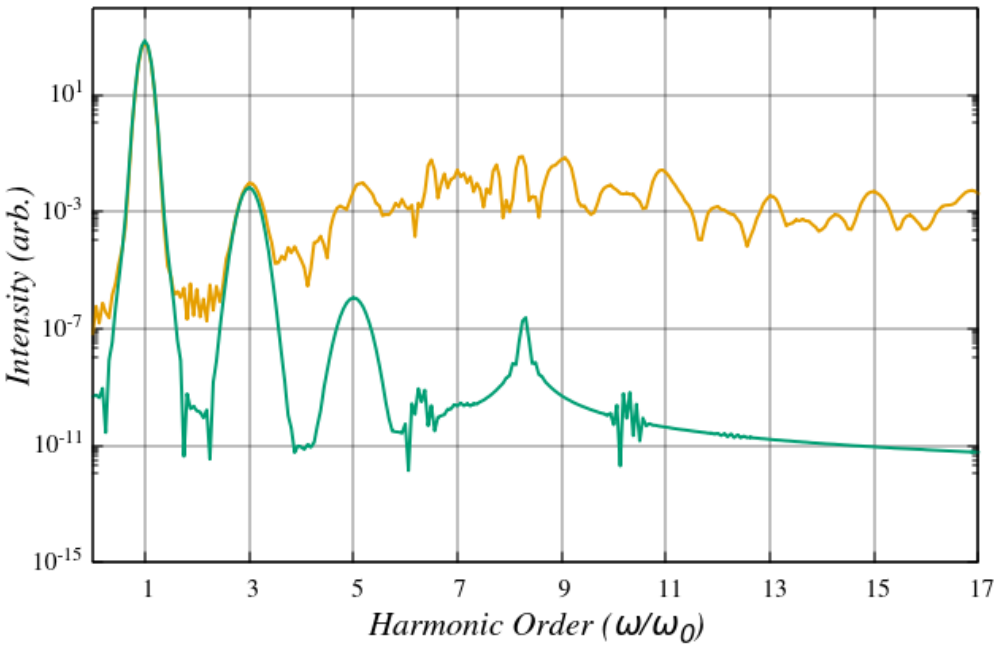


Figure 4: *Comparison of the power spectrum of TDSE (orange curve) with that of the* 4^{th} *order Perturbation (green curve).*

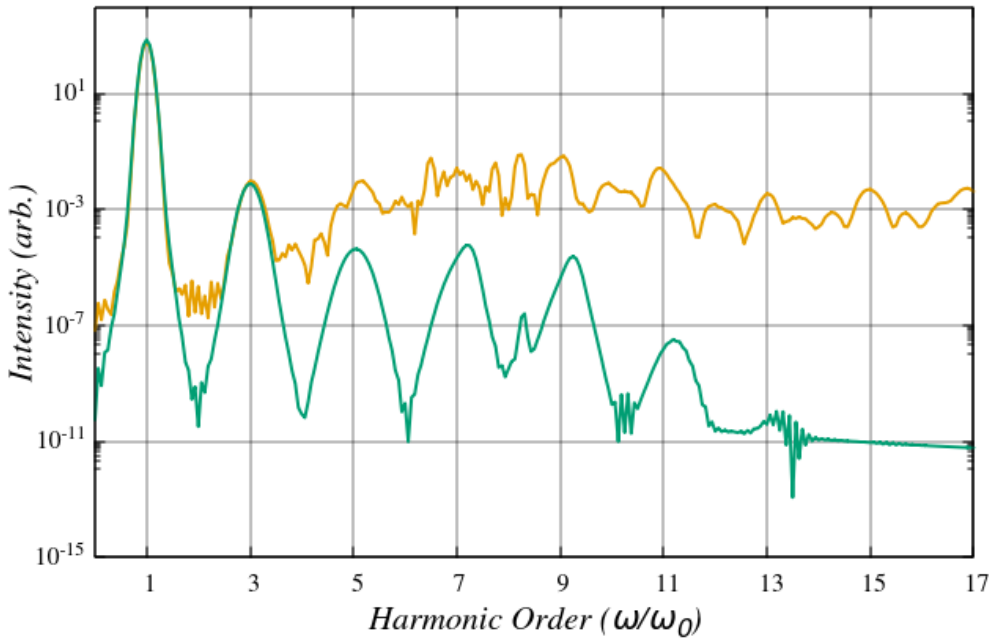


Figure 5: *Comparison of the power spectrum of TDSE (orange curve) with that of the* 8^{th} *order Perturbation (green curve).*

In Figure 3-5, we compared the TDSE results with the 1st order, 4th order, and 8th order perturbations using Green's function method, respectively. The peak laser intensity used in these simulations is $1.0 \times 10^{14} W/cm^2$. We see that the first harmonic in all figures matches the result of the TDSE. That's due to the presence of the electric field term in Eq.104. The driving laser's contribution is inherited in the expectation value of the dipole acceleration via this term. Hence, we see that the correction to the first harmonic is overly dominated by the driving laser. The hydrogen atom requires 9 photons to ionize from its initial state. The ionization rate in TDSE calculation is at $\approx 0.04\%$. The peak at around 9^{th} harmonic can be attributed to the photon energy which is released upon recombination to the initial state. As the order of the perturbation increases, additional harmonics appear. With each additional term in the perturbation, more intermediate states become accessible as seen in Figure 1. We see the resonances of these transitions.

In Figure 6, we show the ratio of time elapsed per order correction to TDSE. The simulations are carried out on Intel® Tiger Lake Core® i5-11400H 6C/12T @ 2.7GHz (Turbo boost 4.5 GHz). processor. We used GNU C compiler version 7.5.0 with O3 switch on.

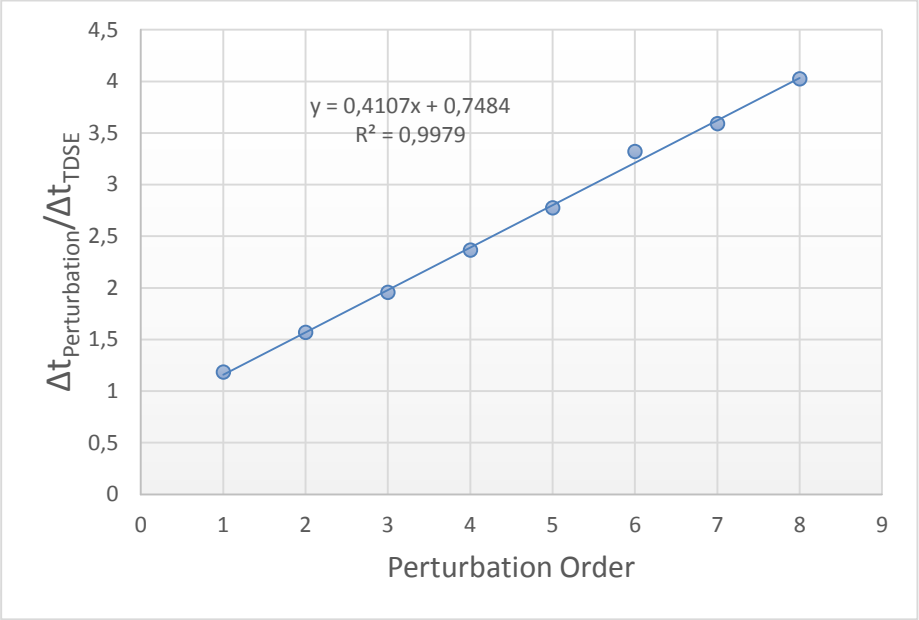


Figure 6: *Ratio of time elapse per perturbation order to TDSE. Trendline is also shown. Each point shown is the outcome of the best of 5.*

3.2. Some Thoughts on Error Propagation

Although theoretically, we can go as many orders as we want, the propagation of error prevents this happening from practical point of view. The maximum possible error can be estimated by assuming that the error accumulates constructively at each iteration. Assuming that only source of error is the truncation error, one may estimate it by the order of the truncation in the approximations. However, due to the complex structure of the algorithms, and behaviors of the approximants, such as Padé approximant, divergence may be considerably slow even beyond the convergence radius. An easier way to test the reliability of the results is the accumulation of error on the first harmonic. The driving laser already dominates the first harmonic considerably. Each correction to the first harmonic should be negligible. If a divergence is detected on the first harmonic, a warnning may be issued to the user.

3.3. Parallelization

The form of the matrix equations (Eq.101, 102, and 103) enables different parallelization schemes. We investigated only one scheme in this study. The CPU time elapsed per correction needs to be balanced with number of terms needed in the partial wave expansion to achieve an optimal parallelization performance. The competition between speed gains due to parallelization and overhead for the preparation of the threads can be challenging. In the case of a confined system, much higher number of terms in the partial wave expansion is needed. Besides, the denser the spatial grid, the better results we get. Denser spatial grid would cause CPU to spend more time in the linear

algebra routines. This enables great performance benefits if architectures such as CUDA is being used [33].

We provide a pseudo code for showing one of the parallelization schemes for the propagator subroutine using *OpenMP* APIs in the next subsection.

3.4.Pseudo Code

#--- CODE BEGINS ---
Set the number of OMP threads
Allocate & initialize radial parts (u_l^n's in Eq. 92 or 95)
OMP parallel region begins
Do for each time step k
    Calculate expectation values
    # First order
    Create OMP thread with only u_l^n *(and intermediates) being shared*
        OMP do for each angular momentum (l)
            Solve Eq.101
        End OMP do
        OMP do for each angular moment (l)
            Solve Eq. 102
        End OMP do
    End OMP thread
    OMP master
        Update wave functions $\Psi(r, t_k)$
    End OMP master
    # Higher orders
    If desired order > 1 then
        Create OMP thread with only u_l^n *(and intermediates) being shared*
            OMP do for each angular momentum (l)
                Solve Eq.101
            End OMP do
            OMP do for each angular moment (l)
                Solve the modified Eq.102 with Eq.103
            End OMP do
        End OMP thread
        OMP master
            Update wave functions $\Psi(r, t_k)$
        End OMP master
    End if
    OMP parallel region ends
    Output expectation values
End do
#--- CODE ENDS ---

4. CONCLUSION

In this study, we have approached HHG simulations with perturbative methods. Green's function method provides a very solid and systematic framework for the solution of perturbative equations. We first developed the matrix equations for our parallel propagator for HHG using the n^{th} order time dependent perturbation theory with Green's functions method, and then developed a parallel code in C programming language using *OpenMP* APIs to simulate HHG that can handle up to the desired perturbation order n. We compared the results of our code with the solution obtained directly from TDSE. We have seen that as the order of the perturbation increases, the peaks generated by our code in the HHG spectrum plots approach to the dominant peaks in the TDSE results. From theoretical point of view, our code is capable of going to any order since Green's function formalism provides easy implementation of recursive functions. However, as we increase the order of perturbation, the numerical stability breaks down due to the error propagation in each iteration and order. We can help the convergence by working on much denser spatial and temporal grids. We can also improve the accuracy using higher order approximants in the theory. However, even with very low-density grids, we managed to approach to the 8^{th} order. However, there is much work needed to be done on the parallelization aspect. We tried to parallelize the matrix equations on CPU using OpenMP. For low densities, the overhead of the preparation of the threads balances the computation time of each matrix equations. A GPU implementation seems to be a better way to parallelize the simulation due to low memory needs of the code, fast thread initialization and GPU's massive number of cores, where each core can handle one term in the partial wave expansion.

REFERENCES

[1] A. McPherson, G. Gibson, H. Jara, U. Johann, T. S. Luk, I. a. McIntyre, K. Boyer, and C. K. Rhodes, *Studies of Multiphoton Production of Vacuum-Ultraviolet Radiation in the Rare Gases*, Journal of the Optical Society of America B **4**, 595 (1987).

[2] P. a. Franken, a. E. Hill, C. W. Peters, and G. Weinreich, *Generation of Optical Harmonics*, Phys Rev Lett **7**, 118 (1961).

[3] J. W. G. Tisch, R. A. Smith, J. E. Muffett, M. Ciarrocca, J. P. Marangos, and M. H. R. Hutchinson, *Angularly Resolved High-Order Harmonic Generation in Helium*, Phys Rev A (Coll Park) **49**, R28 (1994).

[4] J. Peatross and D. D. Meyerhofer, *Angular Distribution of High-Order Harmonics Emitted from Rare Gases at Low Density*, Phys Rev A (Coll Park) **51**, R906 (1995).

[5] J. Peatross and D. D. Meyerhofer, *Intensity-Dependent Atomic-Phase Effects in High-Order Harmonic Generation*, Phys Rev A (Coll Park) **52**, 3976 (1995).

[6] T. Ditmire, E. T. Gumbrell, R. A. Smith, J. W. G. Tisch, D. D. Meyerhofer, and M. H. R. Hutchinson, *Spatial Coherence Measurement of Soft X-Ray Radiation Produced by High Order Harmonic Generation*, Phys Rev Lett **77**, 4756 (1996).

[7] T. Ditmire, J. W. G. Tisch, E. T. Gumbrell, R. A. Smith, D. D. Meyerhofer, and M. H. R. Hutchinson, *Spatial Coherence of Short Wavelength High-Order Harmonics*, Appl Phys B **65**, 313 (1997).

[8] R. Zerne, C. Altucci, M. Bellini, M. B. Gaarde, T. W. Hänsch, A. L'Huillier, C. Lyngå, and C.-G. Wahlström, *Phase-Locked High-Order Harmonic Sources*, Phys Rev Lett **79**, 1006 (1997).

[9] L. le Déroff, P. Salières, and B. Carré, *Beam-Quality Measurement of a Focused High-Order Harmonic Beam*, Opt Lett **23**, 1544 (1998).

[10] T. E. Glover, R. W. Schoenlein, A. H. Chin, and C. v. Shank, *Observation of Laser Assisted Photoelectric Effect and Femtosecond High Order Harmonic Radiation*, Phys Rev Lett **76**, 2468 (1996).

[11] A. Bouhal, R. Evans, G. Grillon, A. Mysyrowicz, P. Breger, P. Agostini, R. C. Constantinescu, H. G. Muller, and D. von der Linde, *Cross-Correlation Measurement of Femtosecond Noncollinear High-Order Harmonics*, Journal of the Optical Society of America B **14**, 950 (1997).

[12] M. Bellini, C. Lyngå, A. Tozzi, M. B. Gaarde, T. W. Hänsch, A. L'Huillier, and C.-G. Wahlström, *Temporal Coherence of Ultrashort High-Order Harmonic Pulses*, Phys Rev Lett **81**, 297 (1998).

[13] Y. Kobayashi, T. Sekikawa, Y. Nabekawa, and S. Watanabe, *27-Fs Extreme Ultraviolet Pulse Generation by High-Order Harmonics*, Opt Lett **23**, 64 (1998).

[14] C.-G. Wahlström, J. Larsson, A. Persson, T. Starczewski, S. Svanberg, P. Salières, Ph. Balcou, and A. L'Huillier, *High-Order Harmonic Generation in Rare Gases with an Intense Short-Pulse Laser*, Phys Rev A (Coll Park) **48**, 4709 (1993).

[15] J. Larsson, E. Mevel, R. Zerne, A. L'Huillier, C.-G. Wahlstrom, and S. Svanberg, *Two-Colour Time-Resolved Spectroscopy of Helium Using High-Order Harmonics*, Journal of Physics B: Atomic, Molecular and Optical Physics **28**, L53 (1995).

[16] Z. Chang, A. Rundquist, H. Wang, I. Christov, H. C. Kapteyn, and M. M. Murnane, *Temporal Phase Control of Soft-x-Ray Harmonic Emission*, Phys Rev A (Coll Park) **58**, R30 (1998).

[17] J. L. Krause, K. J. Schafer, and K. C. Kulander, *High-Order Harmonic Generation from Atoms and Ions in the High Intensity Regime*, Phys Rev Lett **68**, 3535 (1992).

[18] P. B. Corkum, *Plasma Perspective on Strong-Field Multiphoton Ionization*, Phys Rev Lett **71**, 1994 (1993).

[19] I. A. Ivanov and K. T. Kim, *Simple Man Model in the Heisenberg Picture*, Commun

Phys **3**, (2020).
[20] E. Constant, V. D. Taranukhin, A. Stolow, and P. B. Corkum, Methods for the Measurement of the Duration of High-Harmonic Pulses, 1997.
[21] A. Husakou, S.-J. Im, and J. Herrmann, *Theory of Plasmon-Enhanced High-Order Harmonic Generation in the Vicinity of Metal Nanostructures in Noble Gases*, Phys Rev A (Coll Park) **83**, 043839 (2011).
[22] S. Kim, J. Jin, Y.-J. Kim, I.-Y. Park, Y. Kim, and S.-W. Kim, *High-Harmonic Generation by Resonant Plasmon Field Enhancement.*, Nature **453**, 757 (2008).
[23] Y.-Y. Yang, Q.-G. Li, L. Zhang, and X.-C. Lin, *Controlling Plasmonic Field Within Two-Color Laser Using Metallic Nanostructure for Isolated Attosecond Pulse Generation*, Plasmonics **11**, 17 (2016).
[24] J. Choi, S. Kim, I. Y. Park, D. H. Lee, S. Han, and S. W. Kim, *Generation of Isolated Attosecond Pulses Using a Plasmonic Funnel-Waveguide*, New J Phys **14**, (2012).
[25] I. Y. Park, J. Choi, D. H. Lee, S. Han, S. Kim, and S. W. Kim, *Generation of EUV Radiation by Plasmonic Field Enhancement Using Nano-Structured Bowties and Funnel-Waveguides*, Ann Phys **525**, 87 (2013).
[26] I. Yavuz, E. A. Bleda, Z. Altun, and T. Topcu, *Generation of a Broadband Xuv Continuum in High-Order-Harmonic Generation by Spatially Inhomogeneous Fields*, Phys Rev A (Coll Park) **85**, 013416 (2012).
[27] C. Figueira De Morisson Faria and J. M. Rost, *High-Order Harmonic Generation from a Confined Atom*, Phys Rev A **62**, 051402 (2000).
[28] P. Corso, E. Fiordilino, and F. Persico, *Confinement and High-Order Harmonic Generation by a Repulsive Potential*, Phys Rev A (Coll Park) **67**, 063402 (2003).
[29] M. Y. Ivanov and P. B. Corkum, Generation of High-Order Harmonics from Inertially Confined Molecular Ions, 1993.
[30] T. Topcu, E. A. Bleda, and Z. Altun, *Drastically Enhanced High-Order Harmonic Generation from Endofullerenes*, Phys Rev A (Coll Park) **100**, 063421 (2019).
[31] Eleftherios N. Economou, *Green's Functions in Quantum Physics*, 3rd ed. (Springer, 2006).
[32] T. Topçu, TIME-DEPENDENT STUDIES OF FUNDAMENTAL ATOMIC PROCESSES IN RYDBERG ATOMS, 2007.
[33] O. Oguz, Development of High-Order Harmonic Generation Code Using CUDA, Master's Thesis, Marmara University, 2019.
[34] T. Topcu, E. A. Bleda, and Z. Altun, *Drastically Enhanced High-Order Harmonic Generation from Endofullerenes*, Phys Rev A (Coll Park) **100**, 63421 (2019).
[35] Jr. G. A. Baker and P. Graves-Morris, *Padé Approximants* (Cambridge University Press, 1996).
[36] *LAPACK-Linear Algebra PACKage*, https://netlib.org/lapack/.
[37] A. D. Bandrauk, S. Chelkowski, D. J. Diestler, J. Manz, and K. J. Yuan, *Quantum Simulation of High-Order Harmonic Spectra of the Hydrogen Atom*, Phys Rev A **79**, (2009).
[38] *OpenMP*, https://www.openmp.org/.
[39] W. Gropp, E. Lusk, and R. Thakur, *Using MPI-2: Portable Parallel Programming with the Message-Passing Interface*, Vol. 2 (The MIT Press, 1999).
[40] W. Gropp, E. Lusk, A. Skjellum, and R. Thakur, *Using MPI: Portable Parallel Programming with the Message-Passing Interface*, 2nd ed., Vol. 1 (The MIT Press, 1999).
[41] E. A. Bleda, I. Yavuz, Z. Altun, and T. Topcu, *High-Order-Harmonic Generation from Rydberg States at Fixed Keldysh Parameter*, Phys Rev A **88**, 1 (2013).

ÖZGEÇMİŞ

Adı Soyadı : Gökhan İLHAN

İletişim Bilgileri

Mail :

Adres :

ÇEKMEKÖY/İSTANBUL

Doğum Tarihi :

Öğrenim Durumu :

Derece	Alan	Üniversite	Yıl
Lisans	Fizik Bölümü	Marmara Üniversitesi	2011-2015
Lisans	Matematik Bölümü (Ç.A.P.)	Marmara Üniversitesi	2012-2016
Yüksek Lisans	Atom ve Molekül Fiziği	Marmara Üniversitesi	2020 -2023
Doktora			

5. Uluslararası konferanslarda sunulan bildiriler

5.1 lhan, G, Bleda E.A., **"**Green's Function Formalism of nth Order Time-Dependent Perturbation Theory with Improved Accuracy for High-order Harmonic Generation Simulations", Oturum 01OP17, Turkish Physical Society 38th International Physics Congress, 2022

5.2 Ilhan G, Bleda E.A., "Development of a Parallel Green's Function Propagator Algorithm For High-Order Harmonic Generation Simulations", Oturum 01OP12, Turkish Physical Society 37th International Physics Congress, 2021

5.3 Ilhan G, Bleda E.A., "Prediction of Trajectories of 2-Body Problem Using Deep Learning" Oturum 07OP17, Turkish Physical Society 37th International Physics Congress, 2021